


# Intrusive effects of repetitive laser pulsing in high-speed tracer-LIF measurements

M. Papageorge<sup>1</sup> · J. A. Sutton<sup>1</sup> 

Received: 22 December 2016 / Revised: 23 February 2017 / Accepted: 25 February 2017 / Published online: 3 April 2017  
© Springer-Verlag Berlin Heidelberg 2017

**Abstract** The effects of repetitive laser pulsing on laser-induced fluorescence (LIF) signals from three popular organic flow tracers, acetone, 3-pentanone, and biacetyl are examined experimentally in the context of high-speed PLIF imaging. The effects of varying the incident laser fluence, laser repetition rates, tracer mole fractions, and carrier gas (air or N<sub>2</sub>) are investigated. Repetitive laser pulsing leads to changes in the measured LIF signal as a function of laser pulse number for all three tracers. For biacetyl/air mixtures, the LIF signal increases as a function of pulse number and the LIF signal increase per pulse is observed to be a function of the incident laser fluence. For biacetyl/air mixtures at room temperature, the increase in LIF signal during repetitive laser pulsing is attributed solely to absorptive heating of the probe volume, which is confirmed by Rayleigh scattering thermometry measurements. For acetone and 3-pentanone mixtures in the air, the LIF signal decreases with increasing pulse number and the LIF signal depletion per pulse is a linear function of incident laser fluence. This allows the signal depletion per pulse from acetone and 3-pentanone to be normalized by laser fluence and generalized to a single parameter of 0.002%/pulse/(mJ/cm<sup>2</sup>). There is no discernable effect of varying the tracer mole fraction or the laser repetition rate over the range of values investigated. The substitution of N<sub>2</sub> for the air as a carrier gas leads to a significant decrease in the signal depletion per pulse. The potential mechanisms for the enhanced signal depletion in the presence of oxygen are discussed. A likely source is “photo-oxidation”, where the

products of laser photolysis react with the surrounding O<sub>2</sub> to form the highly reactive hydroxyl (OH) radical, which then oxidizes the tracer. Overall, the current results indicate that under repetitive laser pulsing conditions (i.e., high-speed imaging), the tracer-LIF measurement techniques can be considered intrusive unless the laser fluences are kept sufficiently low. The implications for turbulent flow measurements are discussed including recommendations for minimizing the intrusive repetitive pulsing effects.

## 1 Introduction

Laser-induced fluorescence (LIF) of tracer species or “tracer LIF” is a well-established and commonly used approach within the fluid mechanics and combustion fields. For tracer-LIF applications, a well-characterized fluorescing tracer is added to a non-fluorescing fluid and excited with a laser. The emitted light is collected and used to infer certain properties of the local fluid that depends on the relationship between the tracer signal intensity and the environment. For non-reacting fluid mechanics applications, various tracer-LIF approaches have been utilized for monitoring mixing processes (Smith et al. 1998; Picket and Gandhi 2001; Su and Clemens 2003; King et al. 1999; Collins and Jacobs 2002; Weber et al. 2012; Cai et al. 2011), temperature in convective or compressible flows (Kearney and Reyes 2003; Shi et al. 2010; Lee et al. 1993; Thurber and Hanson 2001; Miller et al. 2013; Estruch-Samper et al. 2015; Gamba et al. 2015), and velocity (Koochesfahani and Nocera 2007; ElBaz and Pitz 2012; Danehy et al. 2001, 2003; Zahradka et al. 2016; Lempert et al. 2002; Handa et al. 2014; Reese et al. 2014), while for combustion environments, tracer-LIF approaches have been applied to monitor fuel concentration and mixture fraction

✉ J. A. Sutton  
sutton.235@osu.edu

<sup>1</sup> Department of Mechanical and Aerospace Engineering, Ohio State University, Columbus, USA

(Tait and Greenhalgh 1992; Frank et al. 1994; Sutton and Driscoll 2002, 2006, 2013; Degardin et al. 2006; Galley et al. 2011). In engines, Schulz and Sick (2005) provide a comprehensive review of various popular organic tracer species and tracer-LIF applications that typically include the monitoring of fuel/air ratios (Schulz and Sick 2005; Williams et al. 2010; Blotevogel et al. 2008; Smith et al. 2007) and local thermodynamic conditions such as temperature (Schulz and Sick 2005; Löffler 2010; Rothamer et al. 2010, 2009; Fuyuto et al. 2006; Luong et al. 2008). The review by Schulz and Sick (2005) also provides a comprehensive description of the governing photophysics and details concerning the temperature-, pressure-, and mixture-dependence of the LIF signals from the tracer molecules.

The most common fluorescent tracers include ketones, such as acetone ( $\text{CH}_3\text{COCH}_3$ ), 3-pentanone ( $\text{C}_2\text{H}_5\text{COC}_2\text{H}_5$ ), and biacetyl ( $\text{CH}_3\text{COCOCH}_3$ ); aldehydes, such as acetaldehyde ( $\text{CH}_3\text{CHO}$ ); and aromatic hydrocarbons, such as toluene ( $\text{C}_7\text{H}_8$ ). For each of these species, laser excitation typically occurs in the ultraviolet (UV) regime with red-shifted detection occurring in the UV and visible spectral regions. Because the organic molecules are larger polyatomic species, there is a high density of states and subsequently a broadband absorption spectrum in the UV region. This feature allows the use of common low-repetition-rate pulsed laser sources including the third- (355 nm) and fourth-harmonic (266 nm) output of Nd:YAG lasers and excimer lasers at 248, 308, and 351 nm. The combination of the standard laser sources and red-shifted emission/light collection, which allows simple spectral separation of laser light and fluorescence, has made the aforementioned tracer species not only popular but extensively characterized for their use in fluid, combustion, and engine environments.

Because of its high vapor pressure (185 Torr at 293 K; boiling point = 329.25 K) acetone is an ideal tracer for gas-phase environments. Following the initial demonstrations in isothermal, isobaric environments from Lozano et al. (1992) and Lozano (1992), the number of studies utilizing acetone PLIF have become too numerous to cite with applications ranging from quantitative scalar mixing measurements in canonical flows (i.e., free shear flows such as jets) to practical situations, including engine environments. The attractiveness of acetone as a tracer for quantitative measurements has led to detailed investigations of the tracer's properties, including its temperature- and pressure dependence (Großmann et al. 1996; Yuen et al. 1997; Thurber et al. 1998; Thurber and Hanson 1999; Koch et al. 2004, 2008; Wermuth and Sick 2005; Braeuer et al. 2006). Detailed, multi-step photophysics models of acetone fluorescence yield have been presented (Thurber et al. 1998; Koch et al. 2008, 2004; Wermuth and Sick 2005; Braeuer

et al. 2006) and used to determine species concentrations, temperature, and pressure from various acetone LIF experiments. More recently, 3-pentanone has become a popular ketone tracer, primarily under high-temperature, engine conditions (Rothamer et al. 2009, 2010; Großmann et al. 1996; Koch et al. 2004, 2008; Wermuth and Sick 2005; Braeuer et al. 2006; Cheung and Hanson Wermuth and, b; Modica et al. 2007). Various measurement strategies have been used for monitoring temperature and concentrations, and similar to acetone, detailed temperature and pressure dependences and photophysics models of 3-pentanone fluorescence yield have been developed (Großmann et al. 1996; Koch et al. 2004, 2008; Cheung and Hanson 2012a, b; Modica et al. 2007).

Biacetyl is another aliphatic hydrocarbon fluorescent tracer with extensively studied photophysics and favorable spectroscopic properties [see Schulz and Sick (2005) for comprehensive listing]. Biacetyl has an absorption spectrum that is divided into two bands: one ranging from 210 to 325 nm and a second ranging from 350 to 480 nm. The second absorption band allows access with near-visible and visible lasers as compared to the necessary UV excitation for acetone and 3-pentanone tracers. However, biacetyl has a low room-temperature vapor pressure that prohibits its use under many applications, and as pointed out by Schulz and Sick (2005), biacetyl can suffer from instability problems and exhibits a strong odor. All of these facets may contribute to the lessened popularity as compared to other tracers. Nevertheless, biacetyl has been used as a tracer in many "practical" environments, with the primary application being fuel concentration imaging in engine environments (Smith et al. 2007; Baritaud and Heinze 1992; Deschamps et al. 1994; Smith and Sick 2005a, b; Fajardo et al. 2006; Peterson and Sick 2009; Cundy et al. 2009). While biacetyl has been used quite extensively, its temperature- and pressure dependences are not well documented with only a few studies characterizing temperature and pressure sensitivity under select operating conditions (Wermuth and Sick 2005; Hecklen 1959; Guibert et al. 2002, 2006).

The majority of tracer-LIF measurements have been performed at low-repetition rates, where the high laser pulse energies are quite beneficial to overcome low quantum yield of the tracer's fluorescence process. The combination of high laser pulse energies and low-repetition rates also allows the use of ultra-low-noise and high quantum efficiency scientific CCD cameras, thus greatly increasing measurement resolution and signal to noise. More recently, the emergence of high-speed lasers (i.e., diode-pumped solid state or DPSS lasers) and high-framing-rate cameras has facilitated the possibilities of kHz-rate tracer-LIF measurements. The first applications of high-speed tracer LIF included the work of Sick et al. (2007), Smith and Sick (2005a, b), Fajardo et al. (2006), Peterson and Sick (2009),

Cundy et al. (2009) who utilized biacetyl as a tracer in jet flows and engine environments. Crank-angle resolved fuel concentration measurements in engines (Smith et al. 2007; Smith and Sick 2005a, b; Cundy et al. 2009) and simultaneous scalar/velocity fields in jets and engines (Fajardo et al. 2006; Peterson and Sick 2009) were facilitated with planar laser-induced fluorescence (PLIF) measurements of biacetyl. Excitation of the biacetyl tracer at repetition rates ranging from 4.8 to 12 kHz was performed using the 355-nm output of DPSS Nd:YAG laser with pulse energies  $< 0.5$  mJ, while the PLIF signal was captured using high-speed intensified CMOS cameras. The first quantitative tracer-LIF measurements were reported by Gordon et al. (2009) who used kHz-rate acetone PLIF to measure mixture fraction in an unsteady jet. Subsequently, there have been several applications of high-speed imaging studies using flow tracers in jets, engines, and flames; some examples of which include (Weinkauff et al. 2015; Cundy et al. 2011; Peterson et al. 2013, 2014). An interesting result of the study of Gordon et al. (2009) included some comparisons of signal-to-noise ratio (SNR) and gradient blurring with and without high-speed image intensifiers. Because the output energy from commercial high-speed lasers is somewhat low, high-speed (two-stage) image intensifiers become necessary under many situations to boost signal for low-light applications. Gordon et al. (2009) showed blurring of the measured scalar gradient and recommended measurements to be conducted without image intensifiers when possible. The work by Papageorge et al. (2013) also has shown the effects of the use of high-speed image intensifiers on quantitative scalar measurements, both in terms of gradient blurring, noise effects, and degradation of spatial resolution.

A possible way to circumvent the use of high-speed image intensifiers is to increase the number of collected photons which can come from an increase in the incident laser fluence (energy/area). Irrespective of whether a high-speed image intensifier can be bypassed, an increase in laser fluence can yield an increase in collected signal (and corresponding SNR) as the fluorescence signal is directly proportional to laser fluence (in the absence of saturation or dissociation effects). While the output of commercial DPSS lasers is continually increasing, the recent emergence of pulse burst laser systems (Papageorge et al. 2013; Thurow et al. 2004; Fuest et al. 2012; Slipchenko et al. 2012) offers the opportunity to generate substantial individual pulse energy over a finite “burst” of pulses. For example, Miller et al. (2013a) generated 15 mJ/pulse at 266 nm and demonstrated 10-kHz acetone PLIF imaging in the potential core of a non-reacting jet without the need for an image intensifier. More recent work by Halls et al. (2016) demonstrated the generation of  $\sim 80$  mJ/pulse at 266 nm using a pulse burst laser system. Previous work by the present

authors using the high-energy pulse burst laser (HEPBLs) demonstrated approximately 1 Joule/pulse at 532 nm and 10 kHz (McManus et al. 2015; Papageorge et al. 2014). As will be discussed in the following, this same system leads to 266-nm pulse energies exceeding 145 mJ at 10 kHz. This level of pulse energy is comparable to that obtained with the conventional low-repetition-rate Q-switched laser systems and offers an avenue not only to bypass the need for an image intensifier for planar measurements but to perform tracer-PLIF measurements with low seeding ratios (negligible absorption effects) and still achieve high SNR and spatial resolution.

It is noted that even for low-repetition-rate measurements (where each volumetric element of tracer fluid has a single interaction with the laser probe), higher laser fluence values can pose potential problems due to saturation and/or photolytic effects. In this manner, one must carefully consider the implications for multiple interactions of the tracer fluid with the exciting laser that happens under high-repetition-rate measurements. Two previous studies have investigated the effects of repetitive laser pulsing on targeted measurements. Brusnahan et al. (2013) investigated potential heating by high-repetition-rate laser measurements on surfaces and alterations of the local gas-phase environment. Laser powers up to 63.4 W using a DPSS Nd:YLF laser at 2.4 kHz led to modest surface heating effects, but more importantly, the surface temperatures were found to be directly proportional to the incident laser power. These results indicate that further increases in laser power may lead to significant heating effects and possibly change boundary layer flow properties due to the change in the local thermodynamics. The effects of repetitive pulsing (using a pulse burst laser) on laser-induced incandescence (LII) measurements in flames were investigated by Michael et al. (2015). It was found that the LII signals were sensitive to changes in soot characteristics at high fluence under multi-kHz excitation. Lower laser fluence was required to avoid repetitive probe effects and extract quantitative soot measurements. These studies lead to questions of potential intrusive effects of repetitive laser pulsing during high-speed laser-based measurements; that is, the loss of the implicitly assumed and often touted “non-intrusive”<sup>1</sup> nature of laser-based diagnostics. In this manuscript, we examine the effects of repetitive laser pulsing on measured LIF

<sup>1</sup> The assertion that laser diagnostics are completely “non-intrusive” only is an approximation. In the majority of fluid dynamic applications, the laser-matter interaction results in minimal intrusion that is acceptable to the user in terms of its influence on the fluid-thermochemical state immediately prior to the arrival of the laser pulse. In this manuscript, we refer to this situation as “non-intrusive”. The condition where noticeable laser-induced effects occur is referred to as “intrusive”.

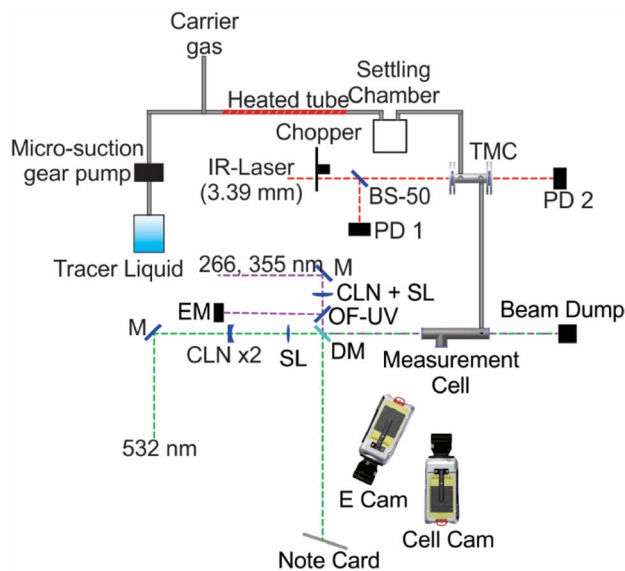


**Fig. 1** Experimental setup for investigating the effects of repetitive laser pulsing on tracer-LIF signals. The setup consists of two primary systems: (1) tracer seeding and monitoring system and (2) optical and imaging system

signals from three popular tracers (acetone, 3-pentanone, and biacetyl) with a particular focus on the effects of incident laser fluence and the implications for *quantitative* scalar measurements.

## 2 Experimental details

The complete experimental configuration for investigating the effects of repetitive laser pulsing on tracer-LIF measurements consists of two primary systems: (1) the tracer seeding and monitoring system and (2) the laser and imaging system. Each of these systems is comprised of multiple subsystems and components, as shown in Fig. 1 and described in detail in the following.

### 2.1 Tracer seeding and monitoring system

The tracer seeding system is designed to deliver a wide variety of volatile liquid tracers to gaseous carrier streams over a wide variety of flow rates and volumetric seeding ratios with high precision and accuracy. The seeding system consists of a carrier gas stream (air or  $N_2$ ), a liquid pump, and an inline heating and temperature control system, as indicated in Fig. 1. Air is supplied from a high-pressure facility line and is filtered through three particle filters to ensure high purity;  $N_2$  (99.998% purity) is supplied from compressed gas cylinders. The carrier gas flow rate is controlled by a mass flow controller (Alicat MCR250), which is user-calibrated with a laminar

flow element. The tracer liquid pump is a micro-suction gear pump (Isamatec ISM901B) with a volumetric flow range of 0.85–85 mL/min and a manufacturer's stated accuracy of  $\pm 0.5\%$  over the full range of flow rates. As shown in Fig. 1, the tracer liquid and carrier gas are mixed together in a long, 3-m, 12.5-mm-diameter tube. To counter the effects of evaporative cooling as the tracer changes from liquid phase to gas phase, the mixing tube is heated and temperature controlled. The temperature control system is combination of a cascade PID control and high-power heating tape that is wrapped around the mixing tube. The temperature of the carrier gas/tracer mixture is measured using a type-K thermocouple in a settling chamber downstream of the mixing tube. To ensure complete evaporation, the set point of the carrier gas/tracer mixture was set to 300 K and was found to be held within  $\pm 0.5$  K after a 15-min transient warmup period.

The carrier gas/tracer mixture is then sent to an optically accessible "tracer monitoring cell" or TMC for a direct and in situ measurement of the tracer concentration (mole fraction). The TMC is a flow-through design, where the carrier gas flow rate is fixed at 21.3 SLPM and the liquid tracer flow rate is adjusted to yield the targeted seeding mole fraction. The TMC is 115 mm long with a 25-mm inner diameter. One 50-mm-diameter calcium fluoride ( $CaF_2$ ) window is mounted on each end for optical measurements of the tracer seed concentration. The tracer monitoring system is based on a direct absorption measurement at  $3.39 \mu\text{m}$  using a 2-mW frequency-stabilized continuous wavelength (CW) infrared (IR) He-Ne laser (Newport Model R-32172). The  $3.39 \mu\text{m}$  output of the He-Ne laser is absorbed by the C-H bonds in the various organic tracers, facilitating a straight forward, but highly accurate concentration measurement. Before entering the TMC, the IR beam is "chopped" using an optical chopper wheel at 800 Hz with a 50% duty cycle to avoid saturation of the detectors and split into two paths using a 50:50 beam splitter (BS-50). The first leg of the  $3.39\text{-}\mu\text{m}$  beam is sent directly into a photodiode (PD1), which serves as a reference measurement, while the remainder of the beam travels through the TMC and then is measured by a second photodiode (PD2). The reference measurement is used to account for any variation in laser power throughout the measurement process. The two detectors (PD1, PD2) are amplified lead selenide (PbSe) photodiodes (Thorlabs PDA-20H) that are sensitive from 1.5 to  $4.8 \mu\text{m}$ . The signal from the two photodiodes is collected using a digital oscilloscope (LeCroy Waverunner 104 MXi; 10 Gs/s, 1 GHz analog bandwidth). Using the Beer-Lambert law, the mole fraction of the tracer ( $X_{\text{tracer}}$ ) is determined from

$$X_{\text{tracer}} = \frac{-\ln\left(\frac{I_{\text{PD2}}^o}{I_{\text{PD2}}^r} \frac{I_{\text{PD1}}^r}{I_{\text{PD1}}^o}\right) R_u T}{L\sigma(\nu) P} \quad (1)$$

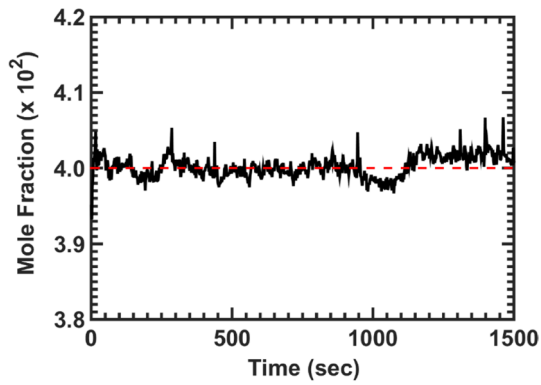


**Fig. 2** Measured acetone mole fraction as a function of time (*solid line*) with a targeted value of 0.04. The *dashed line* shows the average measured acetone mole over the 1500-s measurement period

where  $I/I^0$  is the ratio of the transmitted to incident intensity, subscripts “PD1” and “PD2” refer to the signals collected on detectors PD1 and PD2, respectively,  $L$  is the path length of the absorption cell,  $\sigma(\nu)$  is the frequency-dependent absorption cross section,  $R_u$  is the universal gas constant,  $T$  is the temperature, and  $P$  is the pressure. As an example of the accuracy and precision of the tracer seeding and monitoring system, Fig. 2 shows a sample 1500-s (25-min) trace (*solid black line*) of measured acetone mole fraction with a targeted seeding mole fraction of 0.04. Figure 2 shows that the tracer seeding system was extremely stable with a relative standard deviation of 0.38% over 1500 s and a maximum fluctuation of 1.6% from the mean (shown as red dashed line). Similar stability is noted for the full range of seeding levels considered in this study.

## 2.2 Laser and imaging system

As discussed in Sect. 2.3, two sets of experiments are performed in this study: (a) LIF imaging targeted to understand effects of repetitive laser pulsing on the collected signal and (b) Rayleigh scattering thermometry imaging to investigate local heating effects under repetitive laser pulsing. The optical system consists of (1) two laser systems including the high-energy pulse burst laser system (HEPBLS) outputting 266 and 355 nm for kHz-rate tracer-LIF measurements and a high-speed, 80-W commercial diode-pumped solid-state (DPSS) laser (Edgewave IS80-2-LD) operating at 532 nm for kHz-rate 1D Rayleigh scattering thermometry measurements, (2) two high-framing-rate CMOS cameras, (3) high-speed pulse energy monitoring systems, and (4) an optically accessible “static” measurement cell (MC) for LIF and Rayleigh scattering thermometry monitoring under targeted and controlled conditions.

The HEPBLS is a master oscillator, power amplifier (MOPA) system, where the output of a continuously

operating pulsed, single-frequency fiber laser is amplified in a series of five custom flashlamp-pumped amplifiers. The HEPBLS has been described in previous texts (Papageorge et al. 2013, 2014; Fuest et al. 2012; McManus et al. 2015), so only recent modifications and UV pulse generation are described here. The HEPBLS is a dual-leg system (i.e., two independent outputs) that can operate from 5 to >1000 kHz with burst durations exceeding 25 ms and fundamental (1064-nm) output that exceeds 2.25 J/pulse per leg at 10 kHz. For the current work, repetition rates ranging from 5 to 20 kHz and burst durations up to 20 ms are considered. The second-harmonic (532 nm) output is generated by passing the pulse train through a single  $12 \times 12 \times 20$  mm<sup>3</sup> type I LBO crystal. The third-harmonic output (355 nm) is generated by sending the 1064- and 532-nm output through a dual-wavelength (1064 + 532 nm) waveplate and through a single  $12 \times 12 \times 20$  mm<sup>3</sup> type I LBO crystal. The fourth-harmonic output (266 nm) is generated from the 532-nm output using a  $12 \times 12 \times 2$  mm<sup>3</sup> type I BBO crystal. The thin BBO crystal was selected based on the protocol prescribed by Wu et al. (2000) for high-power 266-nm generation, which minimizes longer term energy drifts and burst-to-burst energy fluctuations. 266-nm pulse energies as high as 145 mJ are achieved from ~800 mJ/pulse at 532 nm at 10 kHz, representing a conversion efficiency of ~17%. As an example of the potential application of the HEPBLS UV output capabilities, Fig. 3 shows an example set of five sequential high-resolution acetone PLIF images acquired at 10 kHz and 70 mJ/pulse from a  $Re = 10,000$  turbulent jet at an axial position of  $x/d = 10$ , where  $d$  is the jet nozzle diameter. The images are extracted from a longer 15-ms (150 sequential images) sequence, and because of the high 266-nm pulse energy, only a high-speed CMOS camera is needed (no image intensifier) for acquisition.

Following the optical schematic in Fig. 1, the UV output (266 or 355 nm depending on the tracer) of the HEPBLS is formed into a 25-mm-tall  $\times$  0.25-mm-thick laser sheet using the combination of an  $f = -300$  mm focal length cylindrical lens and an  $f = 750$  mm focal length spherical lens (CLN + SL). After the SL, an optical flat (OF-UV) is used to pick off a small fraction of the UV laser pulses that is directed to a high-speed energy meter (EM, Ophir PE10-C). The vertically polarized output of the DPSS laser, as directly outputted from the laser head, is  $8 \times 1.6$  mm, which represents an aspect ratio of 5:1. Using a combination of cylindrical lenses, the beam aspect ratio is changed to 1:1 and focused into the test section using an  $f = 750$  mm focal length spherical lens (SL) with a 180  $\mu$ m (FWHM) spot size. Following the SL, an optical flat is used to pick off a small fraction of the 532-nm beam that is directed onto a flat white notecard, where a high-speed CMOS camera (Vision Research Phantom V711), labeled “E Cam”, images the portion of the beam reflecting off of NC, for

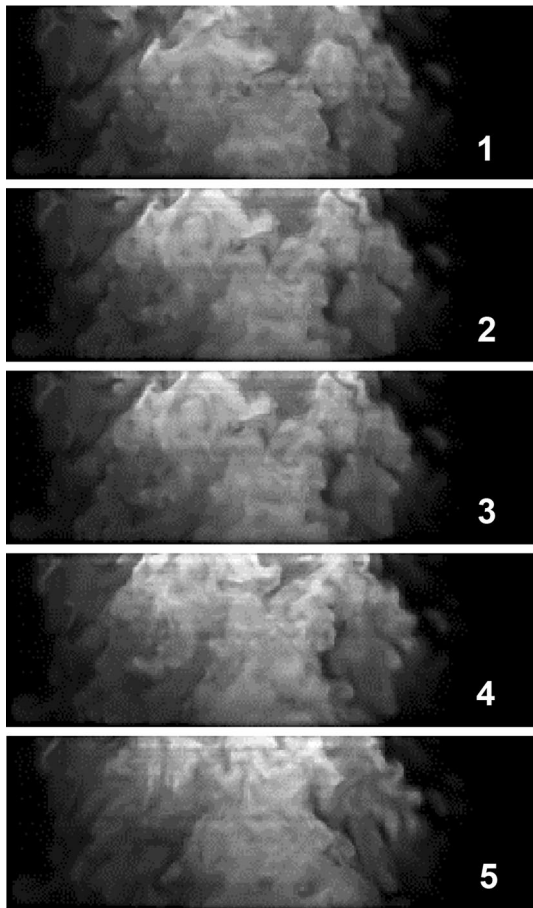


**Fig. 3** Sample 10-kHz acetone PLIF image sequence from a turbulent jet operating at  $Re = 10,000$ . Images are acquired using 70 mJ/pulse at 266 nm. Field-of-view for each image is 11 mm  $\times$  33 mm

relative pulse-to-pulse 532-nm laser energy monitoring. After each of the two optical flats, the UV laser sheet and the 532-nm laser beam are combined using a dichroic mirror (DM). The UV laser sheet and 532-nm laser beam are spatially overlapped using the combination of two high-precision micrometer mounts [placed on the DM and one 532-nm mirror ( $M$ )] and the “knife-edge” method, which leads an overlap which is within  $<30 \mu\text{m}$  at the measurement location.

After flowing through the TMC, the carrier gas/tracer mixture is sent to the optically accessible MC for LIF and Rayleigh scattering measurements. The MC is 260 mm

long with a 48-mm inner diameter and is outfitted with three 50-mm-diameter UV fused silica windows. Two windows are mounted at each end for laser entry and exit and a third viewing window is mounted normal to the optical axis between the entrance and exit windows for imaging access. The kHz-rate PLIF and Rayleigh scattering images are acquired using a high-speed CMOS camera (Vision Research Phantom V711), labeled “Cell Cam” in Fig. 1. For the first set of experiments, only the UV laser sheet is operated and only PLIF images are acquired. For the second set of experiments, both the UV laser sheet and the 532-nm laser are operated simultaneously, but only Rayleigh scattering thermometry images are acquired. For the PLIF measurements, the “Cell Cam” is outfitted with an  $f = 85 \text{ mm } f/1.4$  Nikon camera lens and a magnification of 0.24, such that each pixel has a projected size of  $85 \mu\text{m} \times 85 \mu\text{m}$ . For all measurements, a frame size of  $480 \times 480$  pixels is used, which results in a field-of-view of 41 mm  $\times$  41 mm, which spans the entirety of the useable portion of the MC viewing window. For the 1D Rayleigh imaging measurements, the “Cell Cam” is used in conjunction with the combination of a large 210-mm focal-length,  $f/2.1$  acromat lens, and a 50-mm focal length  $f/1.2$  Nikon camera lens. By combining the acromat with the standard camera lens, the signal collection is maximized for the experimental magnification of 0.22 which leads to a projected pixel size of  $90 \mu\text{m} \times 90 \mu\text{m}$ . For the 1D Rayleigh measurements, a frame size of 512 pixels in the horizontal (beam propagation) direction and 16 pixels in the vertical (normal to the beam propagation) direction is used. Only a small number of pixels are necessary in the vertical direction due to the quasi-1D nature of the Rayleigh scattering “line imaging”.

### 2.3 Data collection and processing

For the tracer-PLIF measurements, three of the most common tracers, acetone ( $\text{CH}_3\text{COCH}_3$ ), 3-pentanone ( $\text{C}_2\text{H}_5\text{COC}_2\text{H}_5$ ), and biacetyl ( $\text{CH}_3\text{COCOCH}_3$ ), are investigated. Table 1 summarizes the various test parameters considered in this study. For measurements at 5 and 10 kHz, the HEPBLS is operated for a burst duration of 20 ms (100 pulses at 5 kHz and 200 pulses at 10 kHz), while for the 20-kHz measurements, the HEPBLS is operated for a burst duration of 10 ms (200 pulses). Figure 4 shows an

**Table 1** Operating parameters

Species	$\lambda_{\text{exc}}$ (nm)	Rep. rate (kHz)	Fluence ( $\text{mJ}/\text{cm}^2$ )	Mole fraction	Carrier gas
Acetone	266	5, 10, 20	13, 67, 133, 190, 266	0.02, 0.04, 0.08	Air, $\text{N}_2$
3-Pentanone	266	10	67, 266	0.035	Air
Biacetyl	355	10	133, 400	0.015	Air

All tests were performed at ambient conditions;  $P = 1 \text{ atm}$ ,  $T = 296 \text{ K}$

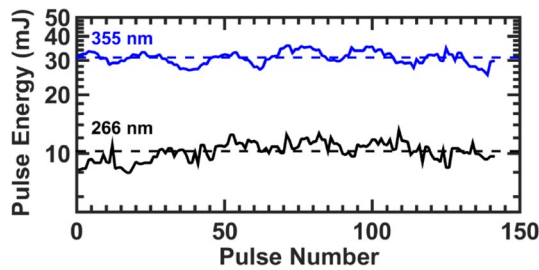


**Fig. 4** Example 355-nm pulse energy trace at an average energy of 30 mJ/pulse or fluence,  $F = 400 \text{ mJ/cm}^2$  (solid blue line) and example 266-nm pulse energy trace at an average energy of 10 mJ/pulse and fluence,  $F = 133 \text{ mJ/cm}^2$  (solid black line). The dashed lines show the average pulse energy for each trace

example 355-nm pulse energy trace at an average energy of 30 mJ/pulse ( $F = 400 \text{ mJ/cm}^2$ ) and an example 266-nm pulse energy trace at an average energy of 10 mJ/pulse ( $F = 133 \text{ mJ/cm}^2$ ) used in the current study. The single-burst relative standard deviation is 7% for the 355-nm output and 10% for the 266-nm output. It should be noted that while the measurements performed in this study utilize a pulse burst laser, the results presented in the manuscript are applicable for any high-speed tracer-LIF measurement, independent of the type of laser source (i.e., pulse burst or DPSS laser). The pulse burst laser is a convenient source for generating high pulse energies, which allows a thorough investigation over a broad range of laser fluence values.

For the high-speed 1D Rayleigh scattering thermometry measurements, the UV output from the HEPBLS and the 532-nm output from the DPSS laser are operated synchronously. The timing of the two laser systems is set, such that 532-nm output from the DPSS laser arrives at the test section  $2 \mu\text{s}$  after the corresponding UV pulse from the HEPBLS to avoid signal interference on the Rayleigh scattering measurements from PLIF emission, since a spectral portion of the fluorescence emission occurs at 532 nm for all tracers considered. The Rayleigh scattering measurements are performed at 10 kHz in the tracer/carrier gas mixtures with and without the HEPBLS output to provide a necessary normalization [see Eq. (3)] and to ensure that any observed effects are due to the presence of the repetitive UV laser pulses. For these measurements, the HEPBLS burst duration is 20 ms, leading to 200 consecutive UV laser pulses. The DPSS laser operates continuously, so the high-speed camera is timed, such that 50 images are recorded immediately prior to the arrival of the first HEPBLS UV laser pulse and 50 pulses are recorded immediately after the arrival of the last HEPBLS UV laser pulse resulting in 300 consecutive Rayleigh scattering images. The 50 images before the HEPBLS burst allow a temperature measurement immediately before repetitive UV excitation and the 50 laser pulses after the HEPBLS burst allow a

temperature measurement after the conclusion of repetitive UV excitation.

For investigating the effects of repetitive laser pulsing on the tracer LIF signal in a controlled manner, it is desired to excite each fluid element with the same number of laser pulses. This is best accomplished with a “static” (no flow) carrier gas/tracer mixture in the MC for each burst of laser pulses. A bypass line is built into the MC to allow the seeding system to operate continuously and constantly flow the carrier gas/tracer mixture while sealing the MC for the measurements, which stagnates the flow inside of the MC. For all measurement cases, 50 bursts of pulses are collected. A burst is collected every 30 s, where following each burst, the MC is opened and the flow is re-routed from the bypass line and flows through the cell for 10 s. The flowrate of the tracer/carrier gas mixture represents ten flow-through times for the 10-s period. This allows the previously “excited” tracer/carrier gas mixture to be purged and replaced with a new tracer/carrier gas mixture. Subsequently, the MC is sealed again and the mixture is allowed 20 s to settle within the MC.

Data processing consists of several steps to ensure accurate results but differs slightly between the PLIF measurements and the Rayleigh thermometry measurements. For the PLIF measurements, the first data processing step consists of removing an average sensor background image (per burst) from each frame of the burst sequence to remove the effects of dark current signal from the camera. This is accomplished by collecting an additional 50 images on the high-speed camera beyond the end of the HEPBLS output. Second, the measured PLIF signal is integrated over all camera sensor rows representing the height of the laser sheet (295 rows) and averaged over a 325-pixel region resulting in a single characteristic signal per image. Third, each signal is corrected by the pulse energy measured with the high-speed energy meter (EM). Figure 4 gives an indication of the level of the pulse-to-pulse energy fluctuation within a single burst. Fourth, each energy-corrected signal is averaged over the 50 pulse bursts to yield an average fluorescence signal per pulse number. Finally, each average signal as a function of pulse number is normalized by the average signal of the first pulse in the burst ( $t = 0$ ).

For the Rayleigh scattering measurements, the first data processing step consists of removing an average sensor background image to remove the effects of dark current signal from the camera. The average background is determined by averaging a set of 300 images collected with both the HEPBLS and DPSS lasers off immediately before and after the 50 data bursts are collected. The second data processing step consists of integrating the measured Rayleigh scattering over all camera sensor rows representing the height of the laser beam (six rows). The third data reduction step involves correcting for pulse-to-pulse laser energy

fluctuations using the “E-Cam” measurement of the reference signal. The fourth data reduction step consists of computing a gas temperature for each pulse within the burst. The measured Rayleigh scattering signal can be written as

$$S_{\text{RAY}} = AI_o N \sigma_{\text{mix}} \quad (2)$$

where  $A$  is a constant describing the collection efficiency of the optics,  $I_o$  is the incident laser intensity,  $N$  is the gas number density, and  $\sigma_{\text{mix}}$  is the mixture-averaged Rayleigh scattering cross section. Using the ideal gas law ( $N = P/kT$ ;  $P =$  pressure,  $k =$  Boltzmann constant) and the consideration of constant pressure and composition, the temperature is determined by

$$T = T_{\text{ref}} \left( \frac{S_{\text{ref}}}{S_{\text{RAY}}} \right) \quad (3)$$

where  $S_{\text{ref}}$  is a reference Rayleigh scattering signal measured from the tracer/carrier gas mixture without the HEP-BLS pulses present at a reference temperature,  $T_{\text{ref}}$  (295 K).  $S_{\text{ref}}$  is determined from the average of ten 300-image bursts collected using the same “purge and refill” procedure described above for the thermometry measurements in the presence of the repetitive UV excitation pulses. The final data reduction steps consist of averaging each temperature (as a function of pulse number) over the 50 bursts.

### 3 Results and discussion

#### 3.1 Acetone, 3-pentanone, and biacetyl: influence of laser fluence

This section examines the influence of varying the incident laser fluence on observed repetitive laser pulsing effects for all three tracers. Acetone ( $\text{CH}_3\text{COCH}_3$ ) and 3-pentanone ( $\text{C}_2\text{H}_5\text{COC}_2\text{H}_5$ ) results are reviewed together as their pressure- and temperature-dependent fluorescence behavior have been shown to be very similar (Koch et al. 2004, 2008; Wermuth and Sick 2005; Cheung and Hanson 2012a, b; Modica et al. 2007).

Figure 5 shows results for the average fluorescence signal ( $S_{\text{fl}}$ ) of an acetone/air mixture as a function of pulse number for a range of laser fluence values varying from 13 to 266  $\text{mJ}/\text{cm}^2$ , which are all within the linear fluorescence regime based on previous work reported within the literature (Lozano 1992). For these measurements, the acetone mole fraction is held constant at 0.04, the repetition rate of the laser is 10 kHz, and the results are normalized by the average fluorescence signal from the first 266-nm laser pulse, denoted as  $S_{\text{fl}}(t = 0)$ . The results show that for all laser fluence values considered, there is a decrease in measured fluorescence signal with increasing number of consecutive laser pulses and the level of signal depletion

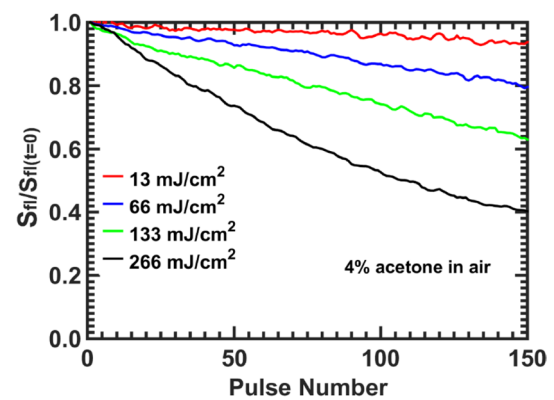


**Fig. 5** Average measured fluorescence signal ( $S_{\text{fl}}$ ) of an acetone/air mixture as a function of pulse number for 266-nm excitation. Results are shown for laser fluence values of 13  $\text{mJ}/\text{cm}^2$  (red line), 66  $\text{mJ}/\text{cm}^2$  (blue line), 133  $\text{mJ}/\text{cm}^2$  (green line), and 266  $\text{mJ}/\text{cm}^2$  (black line). For all results the acetone mole fraction is 0.04 and the laser repetition rate is 10 kHz

from repetitive laser pulsing increases with increasing laser fluence. For the lowest laser fluence considered (13  $\text{mJ}/\text{cm}^2$ ), the signal depletion after 100 pulses (averaged over 50 pulse bursts) is approximately 3% or 0.03% per pulse. For laser fluences of 66, 133, and 266  $\text{mJ}/\text{cm}^2$ , the average signal depletion after 100 consecutive laser pulses is 14, 26, and 48%, respectively. This corresponds to a signal depletion per pulse (SDPP) of 0.14, 0.26, and 0.48% for the 66, 133, and 266  $\text{mJ}/\text{cm}^2$  cases, respectively. As a point of comparison, the SDPP can be considered as an approximation of the level of “signal loss” that would be observed in previous acetone PLIF studies at low-repetition rates. Since the SDPP levels are less than 1%, signal depletion due to laser excitation typically is of little consequence at low-repetition rates. However, at high-repetition rates, where each fluid element has the potential to be subjected to a number of repetitive laser pulses, the cumulative effect can be quite significant, as demonstrated in Fig. 5.

Figure 6 shows results for the average fluorescence signal ( $S_{\text{fl}}$ ) of a 3-pentanone/air mixture as a function of pulse number for laser fluence values of 67 and 266  $\text{mJ}/\text{cm}^2$ , both of which are within the linear fluorescence regime based on previously reported results (Koch 2005). For these measurements, the 3-pentanone mole fraction is held constant at 0.035, the repetition rate of the laser is 10 kHz, and the results are normalized by the average fluorescence signal from the first 266-nm laser pulse, denoted as  $S_{\text{fl}}(t = 0)$ . Similar to the acetone/air results shown in Fig. 5, for each laser fluence case, there is a decrease in the measured 3-pentanone/air mixture fluorescence signal with increasing number of consecutive laser pulses and the level of signal depletion from repetitive laser pulsing increases with increasing laser fluence. For the lower laser fluence



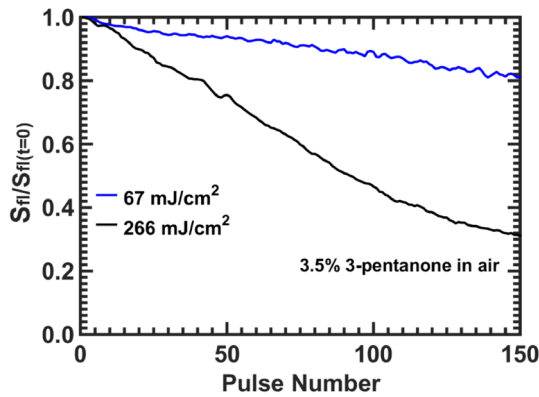


**Fig. 6** Average measured fluorescence signal ( $S_f$ ) of a 3-pentanone/air mixture as a function of pulse number for 266-nm excitation. Results are shown for laser fluence values of 67 mJ/cm<sup>2</sup> (blue line) and 266 mJ/cm<sup>2</sup> (black line). For all results, the 3-pentanone mole fraction is 0.035 and the laser repetition rate is 10 kHz

case (67 mJ/cm<sup>2</sup>), the signal depletion after 100 pulses (averaged over 50 pulse bursts) is approximately 12.5% or SDPP = 0.125%. For the higher fluence case (266 mJ/cm<sup>2</sup>), the average signal depletion is 52% after 100 consecutive laser pulses or an SDPP = 0.52%. Both these SDPP values are within 10% of the values measured for the acetone/air mixture for equivalent laser fluence values. While previous studies have shown that the fluorescence behavior of the two tracers is very similar, the current work extends the tracer comparisons to show that associated signal depletion mechanisms due to repetitive laser pulsing is nearly identical for acetone and 3-pentanone. Because the effects of repetitive laser pulsing on acetone and 3-pentanone mixtures are almost identical, we restrict the detailed reporting of data over a broader range of test conditions (as discussed in Sect. 3.2) to acetone/carrier gas mixtures.

The results of Figs. 5 and 6 appear to indicate a monotonic relationship between laser fluence and signal depletion due to repetitive laser pulsing. Figure 7a shows the combined results of the acetone/air (circle symbols) and 3-pentanone/air (square symbols) mixtures as a function of laser fluence. As shown in Fig. 7a, there is a linear relationship between SDPP (determined from the first 100 laser pulses) and laser fluence for the range of conditions tested. Both tracer/carrier gas mixtures collapse onto the same linear curve. Since SDPP is a linear function of laser fluence, the normalization of the signal depletion per pulse by the incident laser fluence,  $SDPP^* = SDPP/F$ , yields a parameter that collapses all measured values to a single value, as shown in Fig. 7b. For the range of fluence values tested, the current acetone/air and 3-pentanone/air mixtures yield a value of  $SDPP^* = 0.002\%/pulse/(mJ/cm^2)$ . The importance of the results in Figs. 5, 6, and 7 can be viewed in the context of high-speed imaging in turbulent flows, such

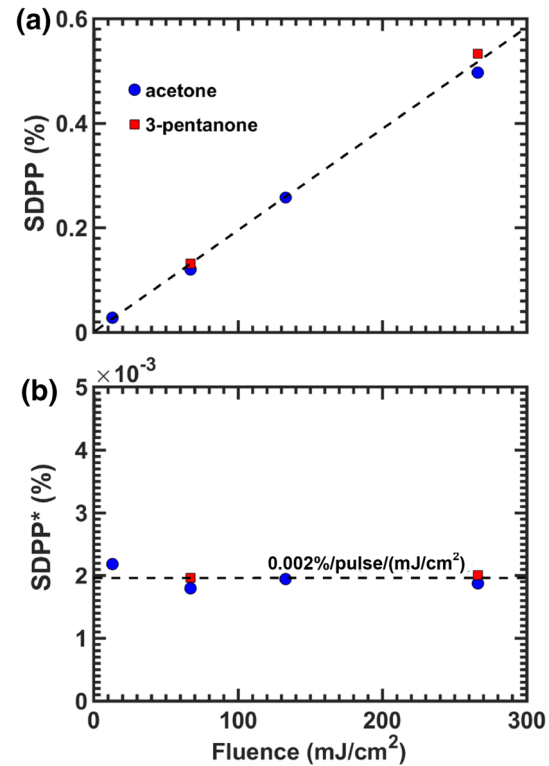


**Fig. 7** **a** Combined results for signal depletion per pulse (SDPP) of the acetone/air (circle symbols) and biacetyl/air (square symbols) mixtures as a function of laser fluence. **b** Normalization of SDPP results by incident laser fluence ( $F$ ) for both the acetone/air (circle symbols) and biacetyl/air (square symbols) mixtures as a function of laser fluence. The normalization yields a parameter  $SDPP^* = SDPP/F$  that collapses all measurements to a single values of  $0.002\%/pulse/(mJ/cm^2)$

as the sample acetone PLIF sequence, as shown in Fig. 3. For the conditions in which the sample image sequence of Fig. 3 was acquired (70 mJ/pulse; 1900 mJ/cm<sup>2</sup>), the expected signal depletion is approximately 3.5% per image. Due to the turbulent nature of the flow, signal depletion at any pixel cannot be distinguished from a decrease in signal due to turbulent mixing or diffusion; that is, signal depletion cannot be determined visually. With signal depletion present, local tracer concentrations inferred from the PLIF images are biased toward lower values yielding erroneous mixing fields.

Figure 10 shows results for the average fluorescence signal ( $S_f$ ) of a biacetyl/air mixture as a function of pulse number for laser fluence values of 133 and 400 mJ/cm<sup>2</sup>. For these measurements, the biacetyl mole fraction is held constant at 0.015, the repetition rate of the laser is 10 kHz, and the results are normalized by the average fluorescence signal from the first 355-nm laser pulse, denoted as  $S_f(t = 0)$ . Contrary to the results shown for the acetone/air and 3-pentanone/air mixtures, the measured fluorescence signal increases within increasing number of consecutive laser

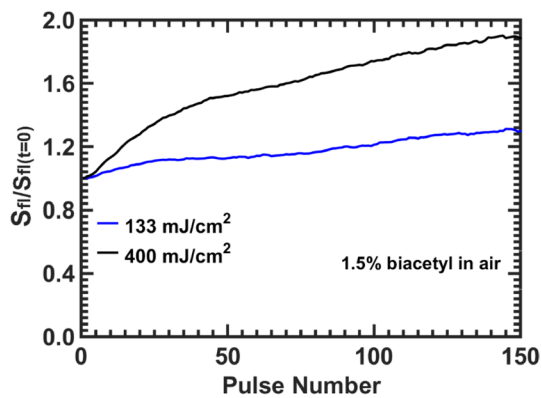


**Fig. 8** Average measured fluorescence signal ( $S_f$ ) of a biacetyl/air mixture as a function of pulse number for 355-nm excitation. Results are shown for laser fluence values of 133 mJ/cm<sup>2</sup> (blue line) and 400 mJ/cm<sup>2</sup> (black line). For all results, the biacetyl mole fraction is 0.015 and the laser repetition rate is 10 kHz

pulses. In addition, the magnitude of the signal increase per pulse (SIPP) increases with increasing laser fluence. The dependence on laser fluence in terms of signal change under repetitive pulsing conditions is consistent with the observations within the acetone/air and 3-pentanone/air mixtures, although signal increase is observed in the biacetyl/air mixtures and signal depletion is observed in the acetone/air and 3-pentanone/air mixtures. The results in Fig. 8 also show that the SIPP continually changes as a function of pulse number. For example, for laser pulses 1 to 35, the average SIPP is approximately 0.35 and 1.25% for  $F = 133$  and 400 mJ/cm<sup>2</sup>, respectively. For laser pulses 35–150, the average SIPP decreases to approximately 0.17 and 0.42% for  $F = 133$  and 400 mJ/cm<sup>2</sup>, respectively. Examining the representative 355-nm laser pulse trace in Fig. 4, the structure of the SIPP as a function of pulse number (Fig. 8) does not appear to be related to the general structure of the laser pulse energy output as a function of time.

### 3.2 Acetone: influence of tracer mole fraction, repetition rate, and carrier gas

Figure 9 shows the effects of varying the acetone mole fraction from 0.02 to 0.08 in the tracer/carrier gas mixture on the average  $S_f$  as a function of pulse number for a single laser fluence of 133 mJ/cm<sup>2</sup>. For these results, the repetition rate of the laser is 10 kHz and the results are normalized by the average fluorescence signal from the first 266-nm laser pulse, denoted as  $S_f(t = 0)$ , for each individual mole fraction case. The results show that the level of signal depletion per pulse can be characterized as nearly independent of acetone mole fraction for the range of mole fractions considered. For example, for the lowest seed level ( $X_{\text{acetone}} = 0.02$ ), the signal depletion due to repetitive laser

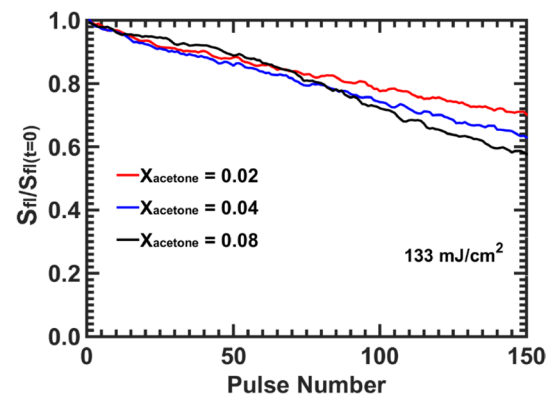


**Fig. 9** Effects of varying acetone mole fraction on the average measured fluorescence signal ( $S_f$ ) for a single laser fluence of 133 mJ/cm<sup>2</sup>. Results are shown for acetone mole fractions of 0.02 (red line), 0.04 (blue line), and 0.08 (black line). For all results, the laser repetition rate is 10 kHz and the excitation wavelength is 266 nm. Results indicate negligible effect of increasing acetone mole fraction over the measured range

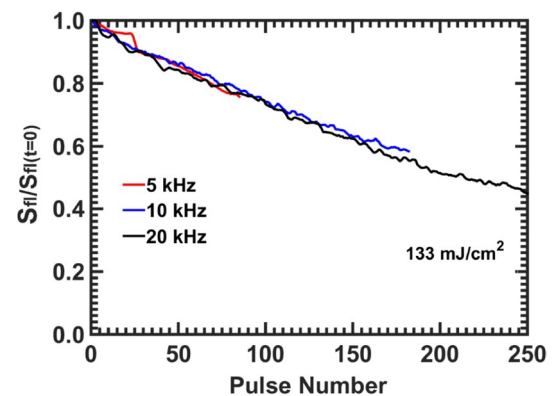


**Fig. 10** Effects of varying laser repetition rate on the average measured fluorescence signal ( $S_f$ ) for a single laser fluence of 133 mJ/cm<sup>2</sup>. Results are shown for repetition rates of 5 kHz (red line), 10 kHz (blue line), and 20 kHz (black line). For all results, the acetone mole fraction is 0.04 and the excitation wavelength is 266 nm. Results indicate negligible effect of increasing laser repetition rate of measured range

pulsing is approximately 23% after 100 laser pulses. For  $X_{\text{acetone}} = 0.04$  and 0.08, the average signal depletion after 100 pulses is 26 and 28%, respectively. This corresponds to SDPP values of 0.23, 0.26, and 0.28% for  $X_{\text{acetone}} = 0.02$ , 0.04, and 0.08, respectively. While the acetone tracer mole fraction changes by 400% over the range of mole fractions considered, the level of signal depletion changes by less than 20% when comparing across the mole fraction cases.

Figure 10 shows the effects of varying the laser repetition rate ( $f$ ) from 5 to 20 kHz on the average  $S_f$  as a function of pulse number. For these results, the acetone mole fraction is 0.04 and the results are normalized by the average fluorescence signal from the first 266-nm laser pulse,

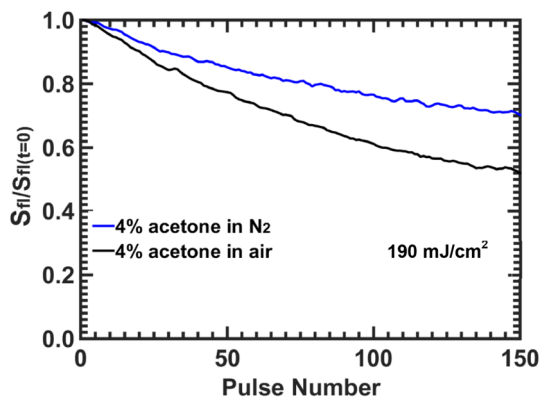


**Fig. 11** Effects of carrier gas on the average measured fluorescence signal ( $S_n$ ) for a single laser fluence of  $190 \text{ mJ/cm}^2$ . Results are shown for nitrogen carrier gas (blue line) and air-carrier gas (black line). For all results, the acetone mole fraction is 0.04, the laser repetition rate is 10 kHz, and the excitation wavelength is 266 nm

denoted as  $S_n(t=0)$ , for each laser repetition rate. Only one laser fluence case of  $133 \text{ mJ/cm}^2$  is shown as results for other fluence values are similar. For the range of laser repetition rates considered in this study, there appears to be no dependence on the actual repetition rate, but rather the total number of pulses ( $N_p$ ) in which the tracer/carrier gas mixture (in a given probe volume) is exposed to. For example, after 85 consecutive pulses, the  $f=5$ -, 10-, and 20-kHz cases are within 1% of each other in terms of total signal depletion ( $\sim 22\%$ ). After 150 pulses, the 10- and 20-kHz cases are within 2% of each other in terms of total signal depletion ( $\sim 38\%$ ). As will be discussed in more detail in Sect. 3.4, we believe that this trend may hold over all repetition rates subject to  $N_p/f \ll \tau_D$ , where  $\tau_D$  is a diffusion timescale of the tracer/carrier gas mixture. As  $N_p/f$  becomes comparable (or larger) than  $\tau_D$ , there is sufficient time for the “excited” tracer/carrier gas mixture to diffuse out of the probe volume and “fresh” tracer/carrier gas mixture to diffuse from the surroundings into the probe volume. Such a process would manifest itself into an observed decrease in (or even an absence of) signal depletion.

Figure 11 shows the effects of changing the carrier gas from the air to pure  $\text{N}_2$  on  $S_n$  as a function of laser pulse number. For these results, the acetone mole fraction is 0.04, the pulse repetition rate is 10 kHz, and the laser fluence is  $190 \text{ mJ/cm}^2$ . The results show a clear dependence of  $S_n/S_n(t=0)$  on the choice of carrier gas with the total signal depletion (and SDPP) being much less when the carrier gas is  $\text{N}_2$  as compared to air. For example, after 100 laser pulses, the total signal depletion for the case of acetone in  $\text{N}_2$  is 24 or 0.24% per pulse, while the total signal depletion for the case of acetone in the air is 39 or 0.39% per pulse. This represents a 60% increase in SDPP when using the air as compared to using  $\text{N}_2$  as a carrier gas. Since the

transport and thermodynamic properties of  $\text{N}_2$  and air are very similar, the results of Fig. 11 may suggest an additional chemical or photo-chemical effect with the presence of  $\text{O}_2$  in the mixture. This will be discussed further in Sect. 3.3.

### 3.3 Possible mechanisms for observed behavior

The results outlined in the previous section identify that repetitive laser pulsing leads to “intrusive” effects, where detected fluorescence signals from the tracer/carrier gas mixture change with an increasing number of consecutive laser pulses. LIF is a process in which an atom or molecule is excited to a higher energy level through the absorption of incident laser photons, followed by the de-excitation of the excited-state species through chemical or physical processes. Chemical processes include photodissociation or photo-chemical reactions. The physical processes typically are characterized as being either radiative (i.e., fluorescence), non-radiative (intra-molecular energy transfer), or collisional quenching (inter-molecular energy transfer). The magnitude of the fluorescence signal is dependent on the (1) local thermodynamic conditions (i.e., temperature and pressure) and (2) rate of chemical, non-radiative, and collisional processes, which also are dependent on the local temperature and pressure. The most probable mechanisms for the change of fluorescence signal as a function of pulse number include a change in the local temperature due to absorptive heating, a photolytic response of the tracer (i.e., dissociation), and/or chemical reactivity of the tracer during the burst of pulses.

To examine the role of heating on the fluorescence signal from biacetyl/air mixtures during repetitive laser pulsing, 1D temperature measurements were performed (simultaneously with the 355-nm excitation source), as outlined in Sects. 3.2 and 3.3. Figure 12a shows the average results from 50 pulse bursts for a 355-nm laser fluence of  $400 \text{ mJ/cm}^2$ . Consistent with the signal increase shown in Fig. 8 (re-plotted as the solid black line in Fig. 12a), the measured gas temperature (solid red line) increases with an increasing number of consecutive pulses. The total measured gas temperature increase is 55 K after 180 pulses at 10 kHz, corresponding to an average heating of 0.31 K/pulse, although the results shown in Fig. 12a clearly show that the heating rate is not uniform. Similar to the signal increase per pulse (SIPP), the rate at which the temperature increases continually changes as a function of pulse number. For laser pulses 1–35, the average heating rate is approximately 0.71 K/pulse, and for laser pulses 35–150, the average heating rate decreases to approximately 0.23 K/pulse. The uncertainty in the average temperature measurements can be estimated by considering the first 60 laser pulses, which corresponds to a static mixture of biacetyl/air at  $\sim 295 \text{ K}$  with no 355-nm

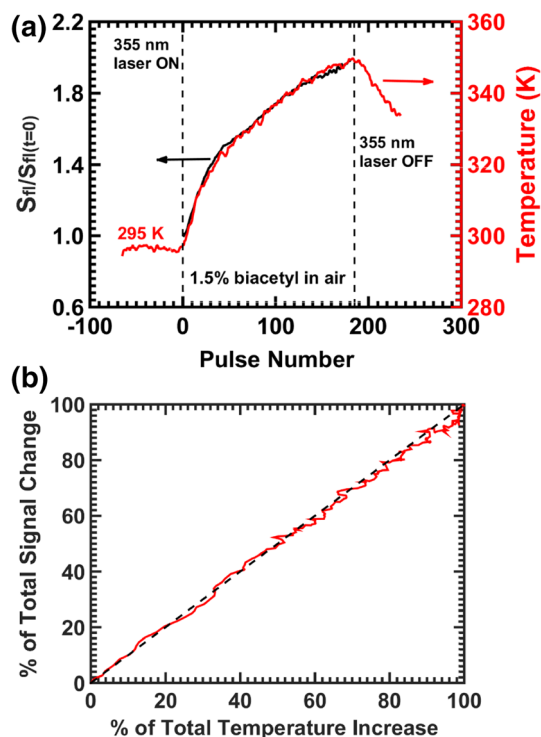


**Fig. 12** **a** Average gas temperature (*solid red line*) of a biacetyl/air mixture as a function of pulse number for a 355-nm laser fluence of  $400 \text{ mJ/cm}^2$ . The *solid black line* shows the results of the average measured fluorescence signal ( $S_{fl}$ ) from Fig. 9. The *two dashed lines* correspond to the “on” and “off” times of the 355-nm excitation laser. **b** Percentage of total biacetyl fluorescence signal increase (*red line*) as a function of the percentage of total measured temperature increase

laser excitation. The difference between the minimum and maximum temperature measured over this span is 2.8 K and the standard deviation is 0.6 K, corresponding to a statistical uncertainty of 0.2%.

Visual inspection of the results shown in Fig. 12a reveals that the structure of  $S_{fl}/S_{fl}(t=0)$  and the gas temperature as a function of pulse number are almost identical, indicating that the SIPP is predominately controlled by the temperature increase per pulse. Figure 12b shows the percentage of the total signal change (solid red line) plotted as a function of the percentage of the total measured temperature increase. The results show a linear relationship (see the dashed black line as a reference) between the two quantities indicating that any change in the measured fluorescence signal is a linear function of the change in the local gas temperature. The results shown in Fig. 12 indicate that the biacetyl fluorescence signal increases at an average rate of 1.8% per degree Kelvin over the range of temperatures considered (295–350 K). This result is compared to the previous results of Guibert et al. (2006), who measured biacetyl fluorescence as a function of temperature, pressure, and composition. At 100 kPa, Guibert et al. (2006) show

results that indicate that the fluorescence signal increases from 373 K to approximately 450 K and then decreases for higher temperatures. At 373 K, the slope of the biacetyl fluorescence as a function of temperature indicates that signal changes by approximately 1.7% per degree K, which is consistent with the current results at lower temperatures. The photo-physics governing the temperature dependence of the biacetyl fluorescence signal is described in Guibert et al. (2006).

While the majority of biacetyl fluorescence applications occur under engine conditions involving temperatures in the range of 500–700 K (Baritaud and Heinze 1992; Deschamps et al. 1994, Smith and Sick 2005a, b; Fajardo et al. 2006; Peterson and Sick 2009; Cundy et al. 2009), the primary utility of the current biacetyl results at lower temperatures demonstrates that repetitive laser pulsing leads to increases in local gas temperatures which are most likely due to absorptive heating. These effects are likely present for all ketone tracers. Under the temperature conditions, representative of engine environments (500–700 K), biacetyl fluorescence, has been shown to be relatively insensitive to temperature changes (Wermuth and Sick 2005; Heicklen 1959; Guibert et al. 2006). Since the primary effect of repetitive laser pulsing at 355 nm on biacetyl/air mixtures is to raise the local gas temperature, kHz-rate measurements using biacetyl as a fluorescent tracer may be possible under engine conditions with acceptable intrusive effects, although this will depend on the particular goal of the experiment.

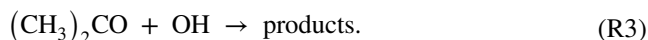
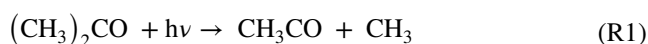
Previous work has shown a strong temperature dependence on the acetone (and 3-pentanone) fluorescence signal. For example, Thurber et al. (1998) showed that the relative fluorescence signal (per unit mole fraction) monotonically decreases with increasing temperature from 300 to 1000 K in acetone/ $\text{N}_2$  mixtures with 266-nm excitation. The relative fluorescence signal was shown to decrease to approximately 50 and 10% of the signal measured at room temperature (295 K) for gas temperatures of 500 and 1000 K, respectively. The temperature dependence arises from the combined effect of decreasing number density and a decreasing fluorescence yield with increasing temperature. Similar to the biacetyl/air mixtures, 1D Rayleigh thermometry was planned in the current acetone and 3-pentanone mixtures to investigate whether gas heating plays a major role in the measured signal depletion shown in Sect. 3. However, during the current kHz-rate measurements within the acetone/air mixtures, significant (and over-whelming) light interference was noted in the measurement volume that did not exist during measurements within the biacetyl/air mixtures. Upon further inspection, it was noted that there was laser damage to the cell windows and a fine particulate coating the cell and windows, both of which will scatter an unacceptable level of 532-nm laser light back to

the measurement volume. Following cleansing of the cell and replacement of the laser windows on the cell, the measurements were attempted again and the same phenomena (apparent particulate formation and subsequent window damage due to the interaction of the laser, particulate, and window) were observed. These results lead to a suspicion of photolytic activity and subsequent chemical reactivity during the repetitive laser pulsing that will be discussed in the following. Due to the damage of the optical windows of the cell, no Rayleigh thermometry measurements were acquired in any of the acetone or 3-pentanone mixtures.

Without accurate thermometry measurements, it is not possible to quantitatively determine the gas heating effects in the acetone and 3-pentanone mixtures. However, since the current results show that the biacetyl/air mixtures are heated due to repetitive laser pulsing, it is expected that the acetone and 3-pentanone mixtures will experience heating effects as well. In fact, the heating effects may be more significant for acetone and biacetyl mixtures, since the absorption cross sections of acetone and 3-pentanone at 266 nm are much larger than the biacetyl absorption cross section at 355 nm. If it is assumed that all of the signal depletions observed in the acetone/N<sub>2</sub> mixture (Fig. 11) are due to gas heating, then the results of Thurber et al. (1998) can be used to estimate the gas temperature and heating rate. After 100 pulses, the 24% decrease in signal shown in Fig. 12 would correspond to a local gas temperature of approximately 385 K or an increase in 90 K over the 100 pulses. This would correspond to an average heating rate of 0.9 K/pulse, which is approximately three times higher than that determined experimentally in the biacetyl/air mixture. Using published absorption cross sections of acetone and biacetyl and the current tracer mole fractions and laser fluence values, a simple energy balance yields an estimated heating rate for the acetone/N<sub>2</sub> mixture that is 3.3 times higher than that of the biacetyl/air mixture. While still speculative at this point, the results suggest that absorptive heating during repetitive laser pulsing plays a significant role in the observed fluorescence signal depletion for ketone tracers when the carrier gas is nitrogen. The relative role of gas heating and other potential depletion sources, such as photodissociation, cannot be determined from the current set of experiments.

When the carrier gas is air, the observed signal depletion increases noticeably as compared to the case, where the carrier gas is N<sub>2</sub> (see Fig. 11). Several studies have shown that for moderate pressures (<3 atm), ketone quantum yield is essentially identical for either N<sub>2</sub> or air-carrier gases (Schulz and Sick 2005; Thurber et al. 1998; Thurber and Hanson 1999), implying that O<sub>2</sub> quenching is very inefficient for lower oxygen partial pressures. In addition, Thurber et al. (1998) showed that fluorescence signals (at 1 atm) in acetone mixtures are the same for N<sub>2</sub> or air

bath gases up to a temperature of 600 K and Ossler and Aldèn (1997) found no detectable differences in acetone fluorescence lifetime with nitrogen or air-carrier gases at 1 atm. Thus, we do not expect that the observed differences between the acetone/N<sub>2</sub> and the acetone/air mixtures are due to enhanced collisional de-excitation or changes in vibrational relaxation (due to the presence of O<sub>2</sub>) with increasing pulse number. The most likely source of increased signal depletion for the acetone/air mixtures as compared to the acetone/N<sub>2</sub> mixtures is chemical reactivity induced by the repetitive laser pulsing. It is well known that photolytic effects (i.e., photodissociation) occur when acetone (or other ketones) is excited with ultraviolet laser pulses (Calvert 1966; Horowitz 1991; Emrich and Warneck 2000; Blitz et al. 2006). While the initial photolytic effects (i.e., (CH<sub>3</sub>)<sub>2</sub>CO + hν → products) are not dependent on the carrier gas, “photo-oxidation” (i.e., photolysis + subsequent oxidation reaction) would only occur in the presence of oxygen. For example, following the initial photolytic reaction (R1), a subsequent reaction channel (R2) will produce the hydroxyl radical (OH) (Emrich and Warneck 2000; Blitz et al. 2006) that can react with acetone (via R3) at low temperatures according to the following sequence:



The reactions of ketones with OH are the primary removal pathways of ketones in the atmosphere. Because of their significant role in atmospheric chemistry, the reaction rate constants of OH radicals with numerous ketones, including acetone and 3-pentanone, have been studied extensively in the temperature range of 250–450 K (Le Calvé et al. 1998; Wollenhaupt et al. 2000; Wallington and Kurylo 1987; Cox 1980). If a mechanism as described by (R1)–(R3) is responsible for the observed behavior, one would expect that with each successive laser pulse, additional CH<sub>3</sub>CO and OH (via R2) is formed. Because the rate of consumption of the acetone (via R3) will scale with the OH concentration, it is expected that the chemical reactivity of acetone will increase with each successive laser pulse. This would manifest itself as an increasing difference between the results of  $S_{fl}/S_{fl}(t=0)$  for the acetone/N<sub>2</sub> case and the acetone/air case with increasing pulse number, which is consistent with the observed behavior (Fig. 11).

The current experimental results provide no direct evidence for the hypothesized reactive process as no measurements of photolytic products or OH are available; however, indirect evidence is available in the form of the aforementioned particle formation during measurements with the

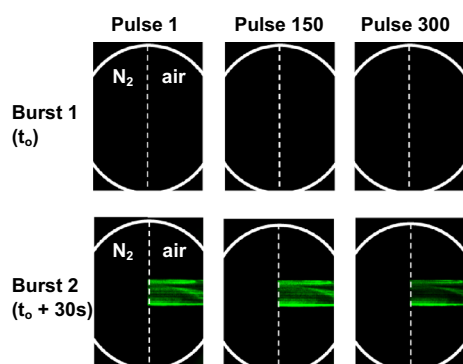


**Fig. 13** Observed particle formation in acetone mixtures using 532-nm laser scattering. *Left* images correspond to acetone/ $N_2$  mixtures and right images correspond to acetone/air images. *Top* Three sample images corresponding to the first, the 150th, and the 300th 532-nm laser pulse immediately following a first burst of 266-nm LIF excitation pulses. *b* Three sample images corresponding to the first, the 150th, and the 300th 532-nm laser pulse immediately following a second burst of 266-nm LIF excitation pulses, 20 s after the first burst. For all results, the acetone mole fraction is 0.04

air. To visualize this phenomenon, the 532-nm laser beam was expanded into a laser sheet to detect particle scattering within the cell. The same experimental protocol as described in Sect. 3.3 was carried out; that is, high-speed imaging from the 532-nm channel was collected simultaneously in the presence of the 266-nm laser sheet. Figure 13 shows the results from two sets of consecutive bursts; one from an acetone/ $N_2$  mixture and one from an acetone/air mixture. The results from the  $N_2$ - and air-carrier gas experiments are combined onto a single image (separated by the white dashed line), where the left half represents the visualization in an  $N_2$  environment and the right half represents visualization in the air environment. The solid white line represents the field-of-view as defined by the observation window. The top row represents the “first bursts” from both the  $N_2$ - and air-carrier gas experiments. Three sample images from each case are shown corresponding to the first, the 150th, and the 300th laser pulse. Neither  $N_2$  nor the air case shows any signs of particle formation. Contrary to the previous experimental protocol defined in Sect. 2.3, the optical cell was not emptied prior to the arrival of another set of 532-nm laser pulses. Sample images from the “second burst”, which occurred 30 s later, are shown in the second row of Fig. 14. As in the first burst, no particle formation is apparent for the  $N_2$  carrier gas case, but significant particle formation is evident for the case with air as the carrier gas as determined by laser light scattering from the particles.

The potential significance of the detected particles has to do with chemistry of the so-called “secondary organic aerosol (SOA)” formation as relevant in atmospheric

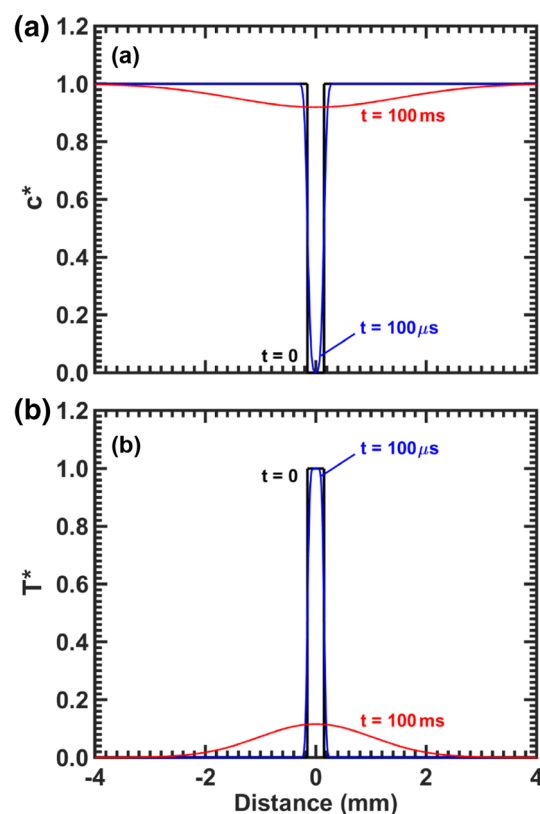


**Fig. 14** Solutions to the 1D diffusion equation to demonstrate the potential for diffusion of heat and species in and out of the laser measurement volume as a function of time. **a** Solutions for normalized concentration,  $c^*$  and **b** solutions for the normalized temperature,  $T^*$ . Results are shown for  $t = 0$  s (black line),  $t = 100 \mu\text{s}$  (blue line), and  $t = 100$  ms (red line)

chemistry research (Kroll and Seinfeld 2008; Hallquist et al. 2009). In SOA, organic compounds (including ketones and other carbonyl compounds from ketone photolysis) are oxidized and the subsequent products which have sufficiently low volatility can condense or nucleate onto preexisting particles (i.e., dust). The most reactive oxidant that initiates oxidation of the organic compounds is OH and it has been shown to be the largest radical initiator of SOA (Kroll and Seinfeld 2008; Hallquist et al. 2009). While the kinetic details of SOA (or other atmospheric chemistry) are well beyond the scope of this paper, the formation of aerosols within the optical cell strongly suggests the presence of OH within the cell when the carrier gas was air. As shown in (R3), the presence of OH allows a direct route to react with the ketones and decrease the local acetone concentration and the acetone fluorescence signal (as compared to the cases with  $N_2$  carrier gas).

### 3.4 Tracer stability: comments on comparisons with previous low-repetition-rate studies

Previous studies have performed photolysis experiments at low laser repetition rates to examine the stability of acetone as a function of the number of laser pulses (Thurber 1999; Bryant et al. 2000). For example, Thurber (1999) examined the reduction of acetone fluorescence signal in a static cell of pure acetone vapor ( $P = 0.05$  atm;  $T = 295$  K) for two laser fluence values of 34 and 84 mJ/cm<sup>2</sup> using 266-nm excitation. Over 12,000 laser shots, the measured acetone fluorescence signal decreased by approximately 5 and 10% for the  $F = 34$  and 84 mJ/cm<sup>2</sup> cases, respectively. Bryant et al. (2000) examined acetone photolysis under atmospheric conditions ( $T = 295$  K) in an acetone vapor/air mixture using 266-nm laser excitation for laser fluence values ranging from 53 to 265 mJ/cm<sup>2</sup>. The results of Thurber (1999) can be interpreted as a SDPP\*  $\sim 1 \times 10^{-5}$  %/pulse/(mJ/cm<sup>2</sup>), while the results of Bryant et al. (2000) show SDPP\* values ranging from  $\sim 4 \times 10^{-6}$  to  $9 \times 10^{-6}$  %/pulse/(mJ/cm<sup>2</sup>). Both these sets of results are qualitatively similar, but are 2.5–3 orders of magnitude less than the values measured in the current study under kHz-rate repetitive laser pulsing. As one point of direct comparison, the  $F = 265$  mJ/cm<sup>2</sup> case of Bryant et al. (2000) in acetone/air at 10 Hz is compared to the  $F = 266$  mJ/cm<sup>2</sup> acetone/air case in the current study. After 10,000 laser pulses, the results from Bryant et al., (Bryant et al. 2000) show a signal depletion of approximately 17%, while for the present results at 10 kHz, a signal depletion of 17% is achieved after only 30 pulses.

The primary difference between the previous stability studies and the current study is the laser repetition rate, i.e., 10 Hz vs. 5–20 kHz, which corresponds to very different time scales between successive laser pulses. For the current kHz-rate measurements, the time between successive laser pulses is 50–200  $\mu$ s, while for the 10-Hz measurements, the time between successive laser pulses is 100 ms, which is  $O(10^3)$  times longer than the kHz-rate measurements. We contend that for the low-repetition-rate measurements, there is sufficient time in between any two successive laser pulses for fluid elements (originally at temperature  $T_0$  and tracer concentration  $c_0$ ) to diffuse away from the probe volume and be “replenished” by “fresh” tracer/carrier gas mixtures from the surroundings. More specifically, assuming that after each laser pulse, fluid elements within the probe volume are heated to a temperature  $T' > T_0$  and the tracer concentration is depleted to a value  $c' < c_0$ , then in the 100-ms interval between laser pulses, the temperature and concentration gradients allow both mass and thermal diffusion to and from the surroundings which are at  $T_\infty < T'$  and  $c_\infty > c'$ .

To qualitatively study this effect, analytical solutions to the 1D diffusion equation ( $\partial\phi/\partial t = \Psi\partial^2\phi/\partial x^2$ ;  $\Psi$  is a diffusion coefficient) are performed for a single slab of fluid of thickness  $\Delta x$  (representing the volume defined by the exciting laser sheet) sandwiched between two infinite slabs of fluid. At time  $t < 0$ ,  $c_0 = c_\infty$  and  $T_0 = T_\infty$  representing a uniform mixture within a given cell at constant temperature. At  $t = 0$ , we assume that the 266-nm laser sheet raises the gas temperature within the laser probe volume to a value  $T' > (T_0 = T_\infty)$  and depletes the concentration in the probe volume to a value  $c' < (c_0 = c_\infty)$ . We then allow the solution to the diffusion equation to evolve in one dimension and in time representing the time between successive pulses for the kHz-rate and Hz-rate cases. To track the heat and mass diffusion in and out of the probe volume, an excess temperature  $T^* = (T - T_\infty)/(T' - T_\infty)$  and a concentration deficit  $c^* = (c - c')/(c_\infty - c')$  are defined. The solutions to the 1D mass ( $\Psi =$  mass diffusivity,  $D$ ) and heat equations ( $\Psi =$  thermal diffusivity,  $\alpha$ ) for  $\Delta x = 300$   $\mu$ m,  $D = 2 \times 10^{-5}$  m<sup>2</sup>/s, and  $\alpha = 5 \times 10^{-6}$  m<sup>2</sup>/s are shown in Fig. 14a and b. The solid black line represents the  $t = 0$  case, where the fluid volume is initially heated and depleted in concentration by some finite amount, corresponding to  $T^* = 1$  and  $c^* = 0$ . The solid blue lines represent the solutions for  $c^*$  and  $T^*$  after 100  $\mu$ s, which corresponds to the inter-pulse spacing for 10-kHz measurements. As shown in Fig. 14a and b, at  $t = 100$   $\mu$ s, negligible concentration from the surroundings has diffused into the probe volume and negligible heat from the probe volume has diffused into the surroundings. We interpret this as a case where the same volume of fluid is being effectively excited by the laser sheet over a large number of consecutive laser pulses. For the case of  $t = 100$  ms (10-Hz excitation), the peak values of  $c^* \sim 0.9$  and  $T^* \sim 0.1$  and both the  $c^*$  and  $T^*$  profiles are significantly broadened showing more than 90% of the heat has diffused away from the probe volume and more than 90% of the depleted tracer concentration has been replenished from the surroundings. This result illustrates that by the time a subsequent laser pulse arrives, significant mass and heat diffusion in and out of the probe volume has occurred and any local gas heating, photolysis, and chemical effects (due to the excitation laser) are not observed due to diffusion effects. It should be noted that true multi-dimensional diffusion effects would likely increase the effective heat loss and tracer replenishment within the probe volume even further. In essence, measurements such as those reported by Thurber (1999) and Bryant et al. (2000) characterize tracer stability in a cell-volume-weighted manner. Because the fluorescence signal is proportional to the tracer mole fraction, inversely proportional to temperature, and proportional to fluorescence yield which increases with decreasing temperature, an order-of-magnitude reduction (due to diffusion) in both the effective heating rate and the tracer

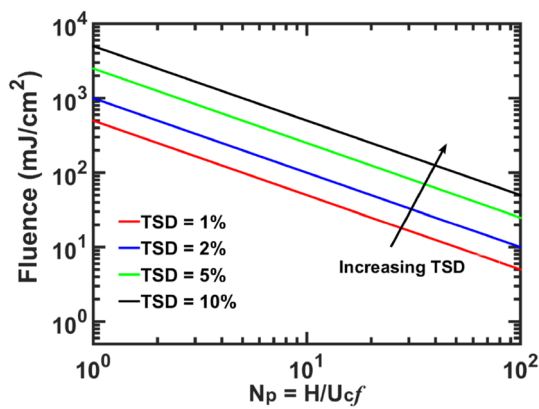


**Fig. 15** Calculations of allowable laser fluence for user-defined total signal depletion (TSD) as a function of the number of laser pulses ( $N_p$ ) that each fluid element encounters. Results are shown for a one-dimensional flow with a single convective velocity

mole fraction depletion rate within the probe volume would correspond to more than two orders-of-magnitude reduction in the measured SDPP, which would be consistent with the tracer stability results measured at low-repetition rates.

#### 4 Recommendations for operation with ketone tracers under turbulent flow conditions

The implications of the results shown in Sect. 3 for the ketone tracers should be interpreted in the context of the number of laser pulses that each fluid element will see in a flowing environment. As a first illustration of this process, we will consider the case of one-dimensional flow with a single convective velocity,  $U_c$ , in the principal flow direction. For a planar imaging experiment with laser sheet height of  $H$ , the number of laser pulses ( $N_p$ ) that each fluid element encounters is  $N_p = H/U_c \times f$ , where  $f$  is the laser repetition rate. For a given set of experimental parameters ( $H, U_c, f$ ), the relationship between laser fluence and total signal depletion (TSD) of the fluid tracer as it convects through the laser sheet is determined from the results shown in Fig. 7, where it was determined that  $SDPP^* = 0.002\%/pulse/(mJ/cm^2)$ . If the practitioner chooses an allowable value of TSD, which represents a *systematic* error, the allowable laser fluence is determined as  $F = TSD / (N_p \times SDPP^*)$ . Figure 15 shows a set of results for allowable laser fluence as a function of  $N_p$  for various values of TSD. As expected, for a given number of laser pulses, the allowable laser fluence increases substantially as the practitioner relaxes the TSD threshold; however, it is noted that as TSD increases, the systematic error of the experiment increases, which can cause difficulty in the proper deduction of flow statistics.

Another observation from Fig. 15 is that for a fixed laser sheet height, the allowable laser fluence is directly proportional to the fluid’s velocity due to the varying number of laser pulses in which the tracer-based fluid elements interact with. This aspect is quite important for turbulent flows for two primary reasons: (1) in general, the mean flow velocity changes with spatial position and (2) the local velocity fluctuates about the mean value giving rise to a distribution of velocities at a given spatial position. In this manner,  $N_p$  fluctuates in both space and time, such that for a general turbulent flow, the number of laser pulses which interact with the tracer fluid is written as

$$N_p(x, t) = Hu(x, t)f \tag{4}$$

where  $\underline{x} = (x_1, x_2)$  represents a 2D position vector<sup>2</sup> with coordinates parallel to and transverse to the laser sheet height,  $H$  and  $u(x, t)$  represent the time-dependent local velocity in the direction parallel with  $H$ . The challenge to this problem lies in determining the maximum allowable fluence, such that an acceptable percentage of measurements in a given spatial region does not exceed a user-determined TSD. Since it is not feasible to change the laser fluence as a function of time, a laser fluence,  $F$  should be chosen, such that

$$\text{probability} \left[ F \leq u(\underline{x}, t) \frac{TSD}{SDPP^*} (Hf)^{-1} \right] \rightarrow 1. \tag{5}$$

This is equivalent to writing

$$F^T = U^T(\underline{x}) \frac{TSD}{SDPP^*} (Hf)^{-1} \tag{6}$$

with the constraint of

$$\text{probability} \left[ U^T(\underline{x}) < u(\underline{x}, t) \right] = \frac{1}{2} \left[ 1 + \text{erf} \left( \frac{M}{\sqrt{2}} \right) \right], \tag{7}$$

where  $F^T$  is a laser fluence suitable for the turbulent flow measurements and  $U^T(\underline{x})$  is a characteristic velocity of the turbulent flow chosen, such that the fluid elements with the lowest velocities are not subject to excessive depletion effects. For turbulent flows that display near-Gaussian statistics, our recommendation is that  $U^T(\underline{x}) = \langle u(\underline{x}, t) \rangle - M\sigma(\underline{x})$ , where  $\langle u(\underline{x}, t) \rangle$  is the mean flow velocity direction parallel with  $H$  at the spatial position  $(x_1, x_2)$ ,  $\sigma(\underline{x})$  is the standard deviation of  $u(\underline{x}, t)$ , commonly known as the RMS fluctuation of  $u(\underline{x}, t)$ , and  $M$  is an integer. Assuming Gaussian statistics, the probability that  $U^T(\underline{x}) < u(\underline{x}, t)$  is

$$\text{probability} \left[ U^T(\underline{x}) < u(\underline{x}, t) \right] = \frac{1}{2} \left[ 1 + \text{erf} \left( \frac{M}{\sqrt{2}} \right) \right], \tag{8}$$

<sup>2</sup> For 2D planar imaging, the third coordinate corresponds to the “out-of-plane” dimension.



which implies that if  $M = 1$ , then the probability that  $U^T(\underline{x}) < u(\underline{x}, t)$  is 0.84 and if  $M = 2$ , then the probability that  $U^T(\underline{x}) < u(\underline{x}, t)$  is 0.98. It is clear that this choice of  $U^T(\underline{x})$  requires knowledge of the flowfield properties. Thus, a second recommendation is that  $\langle u(\underline{x}, t) \rangle$  and  $\sigma(\underline{x})$  are determined a priori for any particular flow configuration in which kHz-rate ketone tracer-PLIF measurements are to be carried out. The preferred method would be to determine  $\langle u(\underline{x}, t) \rangle$  and  $\sigma(\underline{x})$  experimentally, but if experimental velocity measurements are not possible, then suitable estimations of  $\langle u(\underline{x}) \rangle$  and  $\sigma(\underline{x})$  should be made. Appendix demonstrates the constraints that turbulent flows can place on kHz-rate tracer-PLIF measurements by considering the case example of an axisymmetric turbulent jet and the resulting allowable laser fluences for minimizing the repetitive laser pulsing effects.

## 5 Summary and concluding remarks

In this paper, we have examined the effects of repetitive laser pulsing on measured LIF signals of three popular flow tracers, acetone, 3-pentanone, and biacetyl, in the context of high-speed PLIF imaging. For all three tracers, the effects of repetitive laser pulsing led to changes in the LIF signal as a function of pulse number, although the effects were different for biacetyl as compared to the acetone and 3-pentanone. We examined the effects of repetitive laser pulsing with varying levels of laser fluence for all three tracers and examined repetitive laser pulsing effects for various laser repetition rates (5–20 kHz), tracer mole fractions (2–8%), and carrier gas (air or  $N_2$ ) when acetone was the tracer. Overall, the current results indicate that under repetitive laser pulsing conditions (i.e., high-speed imaging), the tracer-LIF measurement techniques can be considered quite intrusive unless the laser fluences are kept sufficiently low.

For biacetyl/air mixtures at room temperature, an increase in LIF signal as a function of laser pulse number was observed, where the signal increase per pulse (SIPP) was a function of the incident laser fluence. The SIPP was attributed solely to local absorptive heating of the probe volume, which was confirmed by Rayleigh scattering thermometry measurements. For the highest fluence used (400 mJ/cm<sup>2</sup>), the average gas heating rate was 0.31 K/pulse when the 355-nm laser was operated at 10 kHz. For room-temperature conditions, the SIPP would prohibit the use of biacetyl as an accurate flow tracer for kHz-rate measurements, but for engine applications with elevated temperatures, the local gas heating may not cause significant unwanted effects as previous works have shown that biacetyl fluorescence is relatively insensitive to temperature changes over the range of 450–550 K.

For the acetone and 3-pentanone tracers in the air, the LIF signal decreased as a function of laser pulse number and the signal depletion per pulse (SDPP) was observed to be a linear function of laser fluence ( $F$ ) over the range of  $F = 13$ –266 mJ/cm<sup>2</sup>. In this manner, the results for both acetone and 3-pentanone collapsed to a single parameter,  $SDPP^* \equiv SDPP/F$ , with a value of  $SDPP^* = 0.002\%/pulse/(mJ/cm^2)$ . The importance of this result becomes clear in the context of high-speed tracer-PLIF imaging, where each tracer-based fluid element interacts with multiple laser pulses and is subject to signal depletion effects. It is further noted that for turbulent flows, the signal depletion cannot be corrected as local changes in signal due to turbulent mixing/diffusion cannot be distinguished from signal depletion. Whenever signal depletion effects are present, local tracer concentrations inferred from PLIF images will be biased towards lower values yielding systematic errors in concentration or mixing measurements.

For acetone, the SDPP was shown to be relatively insensitive to laser repetition rate and tracer mole fraction, but the substitution of  $N_2$  for the air as the carrier gas reduced the SDPP by more than 40% at laser repetition rates of 10 kHz. Thermometry measurements were not available in the acetone mixtures, so it was not possible to discern the relative roles of gas heating and photolytic effects in the acetone/ $N_2$  mixtures. The differences in signal depletion for the acetone/air mixtures as compared to the acetone/ $N_2$  mixtures were most likely due to additional chemical reactivity induced by the repetitive laser pulsing. A likely source is “photo-oxidation”, where the products of laser photolysis react with the surrounding  $O_2$  to form the highly reactive hydroxyl (OH) radical, which then oxidizes the acetone tracer. Evidence of the presence of OH was observed through the detection of fine particulate/aerosol formation in the measurement cell. A well-known (and dominant) aerosol formation pathway relevant in atmospheric chemistry includes the oxidation of organic compounds with OH. Future measurements of OH formation under repetitive laser pulsing conditions would be very beneficial to determine if the aforementioned photo-oxidation mechanism is responsible for the increasing in SDPP when the carrier gas is the air as opposed to  $N_2$ .

Comparisons of previous ketone tracer stability measurements at low-repetition rates (10 Hz) with the current kHz-rate measurements show that the rate of measured LIF signal depletion (or SDPP) is on the order of  $10^2$ – $10^3$  times greater under kHz-rate conditions. Simple analysis considering mass and heat diffusion indicates that the most likely explanation of this discrepancy between low-repetition rate and kHz-rate measurements is the fact that under low-repetition-rate conditions, there is ample time for species and heat to diffuse into and out of the probe volume. In this manner, after a single laser pulse decreases the tracer

species concentration (through photolysis or oxidation) and heats the gas (through absorption), there is sufficient time for diffusion effects to replenish the probe volume with “fresh” gases under low-repetition-rate conditions, thus masking species depletion and heating effects.

Finally, we examined the implications of the ketone signal depletion due to repetitive laser pulsing under turbulent flow conditions. At each point in space and time, the local velocity changes within a turbulent flow which can change the number of laser pulses that each tracer-based fluid element interacts with. Since this phenomenon cannot be predicted a priori, a conservative selection of the laser fluence must be considered to avoid excessive signal depletion effects. We recommend that prior to performing kHz-rate tracer LIF measurements, velocity measurements or velocity estimations are performed in the flow field of interest to characterize the flow statistically. Subsequently a laser fluence should be chosen, such that there is a low probability that a user-determined level of total signal depletion is exceeded due to an excessive number of tracer-pulse interactions arising from velocities that fall below an expected velocity range. In general, regions of low velocity require the application of low laser fluence to avoid signal depletion effects, which will place challenges on achieving an acceptable signal-to-noise ratio (SNR). For high-speed tracer-LIF experiments, the limiting factor of measurement SNR is laser pulse energy (or laser fluence) that minimizes signal depletion effects.

**Acknowledgements** This research was supported by the National Science Foundation (CBET-1336761, Dimitrios Papavassiliou, Program Manager). The authors thank R. Saksena for his help with the analysis of the 1D diffusion problems.

### Appendix: The turbulent axisymmetric jet as a case example for applying kHz-rate tracer-PLIF measurements

To illustrate the constraints that turbulent flows can place on kHz-rate tracer-PLIF measurements, an estimation of allowable laser fluences is performed for turbulent axisymmetric jets of exit velocities  $U_o$  with experimental parameters of  $H = 20$  mm,  $f = 10$  kHz, and  $\text{TSD} = 2\%$ , where it is assumed that the laser sheet is normal to the axial flow direction. The turbulent axisymmetric jet is chosen as an illustrative problem as it is well studied theoretically, is a common experimental platform for tracer-LIF measurements, and demonstrates a large dynamic range of velocities as a function of axial position,  $x$  and radial position,  $r$ . Theoretical solutions for mean velocity field of an axisymmetric jet,  $\langle u(r, x) \rangle$ , are well known and based on the combination of dimensional analysis, solutions to the

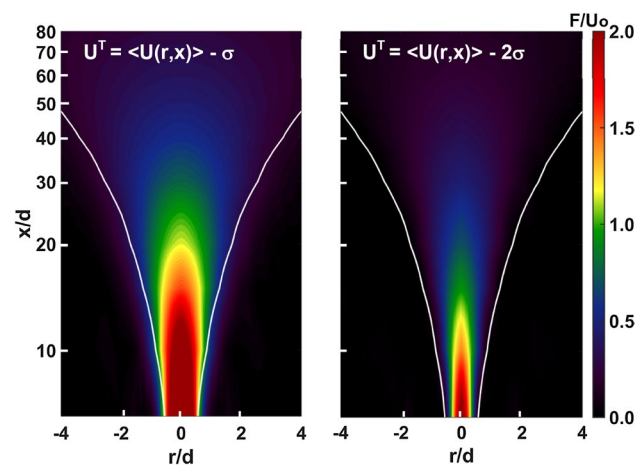


**Fig. 16** Estimations of allowable laser fluence in a turbulent jet as a function of spatial position. **a**  $M = 1$  and **b**  $M = 2$ . For both sets of calculations,  $H = 20$  mm,  $f = 10$  kHz, and  $\text{TSD} = 2\%$ . The local mean axial velocity is determined from theoretical solutions of the velocity field in an axisymmetric turbulent jet and the RMS fluctuation is taken from the data of Wygnanski and Fiedler (1969)

turbulent-boundary layer continuity and momentum equations, and experimental data in the literature (Tacina and Dahm 2000; White and Corfield 2006; Wygnanski and Fiedler 1969). The RMS axial velocity fluctuation (normalized by the centerline axial velocity) is taken from Wygnanski and Fiedler (1969). With both  $\langle u(r, x) \rangle$  and  $u'_{\text{RMS}}(r, x) = \sigma(r, x)$ , it is possible to construct  $U^T(r, x)$  and hence  $F^T(r, x)$  based on Eq. (6).

Figure 16 shows two sets of results for  $F^T/U_o$  for both  $M = 1$  (left) and  $M = 2$  (right) as a function of normalized axial position ( $x/d$ ) and normalized radial position ( $r/d$ ), where  $d$  is the jet nozzle diameter. The fluence,  $F^T$ , is normalized by the jet exit velocity  $U_o$ , such that the result is general for any exit velocity; that is, for constant  $H$  and  $f$ , increasing (or decreasing)  $U_o$  allows an increasing (or decreasing) level of laser fluence for a user-selected TSD. In each figure, the white solid lines represent the FWHM of the jet profile; that is, the radial contour, where the radial velocity is 50% of the centerline velocity or  $r_{1/2}$ . Several observations are evident from the results shown in Fig. 16. First, it is clear that the large dynamic range in velocities in the jet imply a large dynamic range of suitable laser fluence values to avoid excessive signal depletion. For a given experimental field-of-view, a laser fluence should be chosen that corresponds to the lowest expected  $U^T$  in the field-of-view. To maximize  $F^T$  for a given spatial region, this facet promotes a small field-of-view, which greatly reduces spatial dynamic range and increases the amount of experimental data that must be collected. Second, it is noted that for a given exit velocity,  $U_o$ ,  $F^T \rightarrow 0$  as  $x \rightarrow \infty$  and  $r \rightarrow \pm\infty$ , since the local velocity,  $u(r, x) \rightarrow 0$ . As the

collected signal is directly proportional to  $F^T$ , the signal-to-noise ratio (SNR) of the measurement will be proportional to  $\sqrt{F^T}$  under shot-noise-limited conditions. In this manner, there exists some axial and radial position, where the measurements are not feasible due to the competition between SNR and TSD. For example, upon examining the  $M = 2$  case (right image of Fig. 16), it is noted that  $F^T \rightarrow 0$  well before the  $r_{1/2}$  contour, thus relegating potential kHz-rate tracer-LIF measurements to near-centerline and upstream axial locations. Obviously, the TSD threshold could be increased to increase the measurement domain, but this will lead to a larger level of systematic error in the kHz-rate tracer-LIF measurements. Third, it is noted that while the  $M = 2$  case yields a higher probability that  $U^T(r, x) < u(r, x)$ , the range of spatial locations in which measurements with suitable SNR (as assumed through the  $\sqrt{F^T}$  dependence) will be possible is significantly reduced as compared to the  $M = 1$  case. However, the  $M = 1$  case will exhibit a higher probability that  $U^T(r, x) > u(r, x)$ , thus increasing the systematic error of the kHz-rate measurements.

While the results shown in Fig. 16 are not indicative of all experimental configurations, they do show that because of signal depletion effects from repetitive laser pulsing, the laser fluence must be kept at a suitably low levels, which may change as the local velocity and velocity fluctuations change. A general observation is that as local velocities decrease, each fluid element is subjected to an increasingly higher number of laser pulses (for given sheet height,  $H$ ), which dictates that the chosen  $F^T$  (necessary to maximize collected signal) needs to decrease and may render certain measurements or measurement locations unfeasible. The current results also indicate that while systems such as pulse burst laser systems have demonstrated very high laser energies, under many experimental configurations, the output typical of DPSS lasers is appropriate to minimize signal depletion effects due to repetitive laser pulsing. However, it should be noted that the ability to generate high laser pulse energies from pulse burst laser systems can be utilized in additional ways. For example, pulse burst systems still offer the ability to go to ultrahigh-repetition rates if such an experiment (i.e., high-speed turbulent flow) dictates this need. For example, for a laser fluence of  $10 \text{ mJ/cm}^2$  ( $\sim 1 \text{ mJ}$  in a  $30 \text{ mm} \times 0.3 \text{ mm}$  laser sheet), it is expected that the current HEPBLS (used to generate the results in Fig. 1) could operate with 266-nm output at repetition rates exceeding 500 kHz.

## References

- Baritaud TA, Heinze TA (1992) Gasoline distribution measurements with PLIF in a SI engine, SAE Technical Paper 922355
- Blitz MA, Heard DE, Pilling MJ (2006) Study of acetone photodissociation over the wavelength range 248–330 nm: Evidence of a mechanism involving both the singlet and triplet excited states. *The J Phys Chem A* 110(21):6742–6756
- Blotevogel T, Hartmann M, Rottengruber H, Leipertz A (2008) Tracer-based laser-induced fluorescence measurement technique for quantitative fuel/air-ratio measurements in a hydrogen internal combustion engine. *Appl Opt* 47(35):6488–6496
- Braeuer A, Beyrau F, Leipertz A (2006) Laser-induced fluorescence of ketones at elevated temperatures for pressures up to 20 bars by using a 248 nm excitation laser wavelength: experiments and model improvements. *Appl Opt* 45(20):4982–4989
- Brusnahan M, Lu L, Sick V (2013) Parasitic heating effects in high frame rate laser imaging experiments. *Appl Phys B* 111(4):651–658
- Bryant RA, Donbar JM, Driscoll JF (2000) Acetone laser induced fluorescence for low pressure/low temperature flow visualization. *Exp Fluids* 28(5):471–476
- Cai J, Dinger MJ, Li W, Carter CD, Ryan MD, Tong C (2011) Experimental study of three-scalar mixing in a turbulent coaxial jet. *J Fluid Mech* 685:495–531
- Calvert JG, Pitts Jr JN (1966) *Photochemistry*, vol 8. Wiley, New York, p 99
- Cheung BH, Hanson RK (2012a) 3-pentanone fluorescence yield measurements and modeling at elevated temperatures and pressures. *Appl Phys B* 106(3):755–768
- Cheung BH, Hanson RK (2012b) Determination of fluorescence and non-radiative de-excitation rates of excited 3-pentanone at low pressures. *Appl Phys B* 106(3):741–753
- Collins BD, Jacobs JW (2002) PLIF flow visualization and measurements of the Richtmyer–Meshkov instability of an air/SF6 interface. *J Fluid Mech* 464:113–136
- Cox RA, Derwent RG, Williams MR (1980) Atmospheric photooxidation reactions. Rates, reactivity, and mechanism for reaction of organic compounds with hydroxyl radicals. *Environ Sci Tech* 14(1):57–61
- Cundy M, Schucht T, Thiele O, Sick V (2009) High-speed laser-induced fluorescence and spark plug absorption sensor diagnostics for mixing and combustion studies in engines. *Appl Opt* 48(4):B94–B104
- Cundy M, Trunk P, Dreizler A, Sick V (2011) Gas-phase toluene LIF temperature imaging near surfaces at 10 kHz. *Exp Fluids* 51:1169–1176
- Danehy PM, Mere P, Gaston MJ, O’Byrne S, Palma PC, Houwing AFP (2001) Fluorescence velocimetry of the hypersonic, separated flow over a cone. *AIAA J* 39(7):1320–1328
- Danehy PM, O’Byrne S, Houwing, A.F.P., Fox JS, Smith DR (2003) Flow-tagging velocimetry for hypersonic flows using fluorescence of nitric oxide. *AIAA J* 41(2):263–271
- Degardin O, Renou B, Boukhalfa AM (2006) Simultaneous measurement of temperature and fuel mole fraction using acetone planar induced fluorescence and Rayleigh scattering in stratified flames. *Exp Fluids* 40(3):452–463
- Deschamps B, Snyder R, Baritaud T (1994) Effect of flow and gasoline stratification on combustion in a 4-valve SI engine, SAE Paper 941993
- EIBaz AM, Pitz RW (2012) N<sub>2</sub>O molecular tagging velocimetry. *Appl Phys B* 106(4):961–969
- Emrich M, Warneck P (2000) Photodissociation of acetone in air: Dependence on pressure and wavelength. Behavior of the excited singlet state. *J Phys Chem A* 104(42):9436–9442
- Estruch-Samper D, Vanstone L, Hillier R, Ganapathisubramani B (2015) Toluene-based planar laser-induced fluorescence imaging of temperature in hypersonic flows. *Exp Fluids* 56:115

- Fajardo CM, Smith JD, Sick V (2006) Sustained simultaneous high-speed imaging of scalar and velocity fields using a single laser. *Appl Phys B* 85(1):25–30
- Frank JH, Lyons KM, Marran DF, Long MB, Starner SH, Bilger RW (1994) Mixture fraction imaging in turbulent nonpremixed hydrocarbon flames. *Proc Combust Inst* 25:1159–1166
- Fuest F, Papageorge MJ, Lempert WR, Sutton JA (2012) Ultrahigh laser pulse energy and power generation at 10 kHz. *Opt Lett* 37(15):3231–3233
- Fuyuto T, Kronemayer H, Lewerich B, Koban W, Akihama K, Schulz C (2006) Laser-based temperature imaging close to surfaces with toluene and NO-LIF. *J Phys Conf Ser* 45:69–76
- Galley D, Ducruix S, Lacas F, Veynante D (2011) Mixing and stabilization study of a partially premixed swirling flame using laser induced fluorescence. *Combust. Flame* 158(1):155–171
- Gamba M, Miller VA, Mungal MG, Hanson RK (2015) Temperature and number density measurement in non-uniform supersonic flowfields undergoing mixing using toluene PLIF thermometry. *Appl Phys B* 120(2):285–304
- Gordon RL, Heeger C, Dreizler A (2009) High-speed mixture fraction imaging. *Appl Phys B* 96(4):745–748
- Großmann F, Monkhouse PB, Ridder M, Sick V, Wolfrum J (1996) Temperature and pressure dependencies of the laser-induced fluorescence of gas-phase acetone and 3-pentanone. *Appl Phys B* 62:249–253
- Guibert P, Perrard W, Morin C (2002) Concentration measurements in a pressurized and heated gas mixture flow using laser induced fluorescence. *J Fluids Eng* 124:512–522
- Guibert P, Modica V, Morin C (2006) Influence of pressure, temperature and gas phase composition on biacetyl laser-induced fluorescence. *Exp Fluids* 40(2):245–256
- Hallquist M, Wenger JC, Baltensperger U, Rudich Y, Simpson D, Claeys M, Hamilton J (2009) F., The formation, properties and impact of secondary organic aerosol: current and emerging issues. *Atm Chem Phys* 9(14):5155–5236
- Halls BR, Gord JR, Meyer TR, Thul DJ, Slipchenko M, Roy S (2016) 20-kHz-rate three-dimensional tomographic imaging of the concentration field in a turbulent jet. *Proc Combust Inst*. doi:10.1016/j.proci.2016.07.007
- Handa T, Mii K, Sakurai T, Imamura K, Mizuta S, Ando Y (2014) Study on supersonic rectangular microjets using molecular tagging velocimetry. *Exp Fluids* 55(5):1–9
- Heicklen J (1959) The fluorescence and phosphorescence of biacetyl vapor and acetone vapour. *J Am Chem Soc* 81:3863–3866
- Horowitz A (1991) Wavelength dependence of the primary photodissociation processes in acetone photolysis. *J Phys Chem* 95(26):10816–10823
- Kearney S, Reyes F (2003) Quantitative temperature imaging in gas-phase turbulent thermal convection by laser-induced fluorescence of acetone. *Exp Fluids* 34(1):87–97
- King GF, Lucht RP, Dutton JC, Instantaneous (1999) Quantitative measurements of molecular mixing in the axisymmetric jet near field. *Phys Fluids* 11(2):403–416
- Koch J (2005) Fuel tracer photophysics for quantitative planar laser-induced fluorescence. Ph. D. Dissertation, Stanford University
- Koch JD, Hanson RK, Koban W, Schulz C (2004) Rayleigh-calibrated fluorescence quantum yield measurements of acetone and 3-pentanone. *Appl Opt* 43(31):5901–5910
- Koch JD, Gronki J, Hanson RK (2008) Measurements of near-UV absorption spectra of acetone and 3-pentanone at high temperatures. *J Quant Spec Rad Trans* 109(11):2037–2044
- Koochesfahani MM, Nocera DG, Foss J, Tropea C, Yarin A (2007) Molecular tagging velocimetry. In: *Handbook of experimental fluid dynamics*
- Kroll JH, Seinfeld JH (2008) Chemistry of secondary organic aerosol: formation and evolution of low-volatility organics in the atmosphere. *Atm Environ* 42(16):3593–3624
- Lozano A (1992) Laser-excited luminescent tracers for planar concentration measurements in gaseous jets. Ph. D. Dissertation, Stanford University
- Lozano A, Yip B, Hanson RK (1992) Acetone: a tracer for concentration measurements in gaseous flows by planar laser-induced fluorescence. *Exp Fluids* 13(6):369–376
- Le Calvé S, Hitier D, Le Bras G, Mellouki, A (1998) Kinetic studies of OH reactions with a series of ketones. *J Phys Chem A* 102(24):4579–4584
- Lee MP, McMillin BK, Hanson RK (1993) Temperature measurements in gases by use of planar laser-induced fluorescence imaging of NO. *Appl Opt* 32(27):5379–5396
- Lempert WR, Jiang N, Sethuram S, Samimy M (2002) Molecular tagging velocimetry measurements in supersonic microjets. *AIAA J* 40(6):1065–1070
- Löffler M, Beyrau F, Leipertz A (2010) Acetone laser-induced fluorescence behavior for the simultaneous quantification of temperature and residual gas distribution in fired spark-ignition engines. *Appl Opt* 49(1):37–49
- Luong M, Zhang R, Schulz C, Sick V (2008) Toluene laser-induced fluorescence for in-cylinder temperature imaging in internal combustion engines. *Appl Phys B* 91:669–675
- McManus TA, Papageorge MJ, Fuest F, Sutton JA (2015) Spatio-temporal characteristics of temperature fluctuations in turbulent nonpremixed jet flames. *Proc Combust Inst* 35(2):1191–1198
- Michael JB, Venkateswaran P, Shaddix CR, Meyer TR (2015) Effects of repetitive pulsing on multi-kHz planar laser-induced incandescence imaging in laminar and turbulent flames. *Appl Opt* 54(11):3331–3344
- Miller JD, Michael JB, Slipchenko MN, Roy S, Meyer TR, Gord JR (2013a) Simultaneous high-speed planar imaging of mixture fraction and velocity using a burst-mode laser. *Appl Phys B* 113:93–97
- Miller VA, Gamba M, Mungal MG, Hanson RK (2013b) Single- and dual-band collection toluene PLIF thermometry in supersonic flows. *Exp Fluids* 54:1539
- Modica V, Morin C, Guibert P (2007) 3-Pentanone LIF at elevated temperatures and pressures: measurements and modeling. *Appl Phys B* 87(1):193–204
- Ossler F, Alden M (1997) Measurements of picosecond laser induced fluorescence from gas-phase 3-pentanone and acetone: implications to combustion diagnostics. *Appl Phys B* 64:493–502
- Papageorge MJ, Arndt C, Meier W, Sutton JA (2014) High-speed mixture fraction and temperature imaging of pulsed, turbulent fuel jets auto-igniting in high-temperature, vitiated co-flows. *Exp Fluids* 55:1763
- Papageorge MJ, McManus TA, Fuest F, Sutton JA (2013) Recent advances in high-speed planar Rayleigh scattering in turbulent jets and flames: increased record lengths, acquisition rates, and image quality. *Appl Phys B* 115(2):197–213
- Peterson B, Sick V (2009) Simultaneous flow field and fuel concentration imaging at 4.8 kHz in an operating engine. *Appl Phys B* 97:887–895
- Peterson B, Baum E, Boehm B, Sick V, Dreizler A (2013) High-speed PIV and LIF imaging of temperature stratification in an internal combustion engine. *Proc Combust Inst* 34:3653–3660
- Peterson B, Baum E, Bohm B, Sick V, Dreizler A (2014) Evaluation of Toluene LIF Thermometry detection strategies applied in an internal combustion engine. *Appl Phys B* 117:151–175
- Picket LM, Ghandhi JB (2001) Passive scalar measurements in a planar mixing layer by PLIF of acetone. *Exp Fluids* 31(3):309–318
- Reese D, Oakley J, Navarro-Nunez A, Rothamer D, Weber C, Bonazza R (2014) Simultaneous concentration and velocity field

- measurements in a shock-accelerated mixing layer. *Exp Fluids* 55:1823
- Rothamer DA, Snyder JA, Hanson RK, Steeper RR, Fitzgerald RP (2009) Simultaneous imaging of exhaust gas residuals and temperature during HCCI combustion. *Proc Combust Inst* 32(2):2869–2876
- Rothamer DA, Snyder JA, Hanson RK, Steeper RR (2010) Optimization of a tracer-based PLIF diagnostic for simultaneous imaging of EGR and temperature in IC engines. *Appl Phys B* 99(1):371–384
- Schulz C, Sick V (2005) Tracer-LIF diagnostics: quantitative measurement of fuel concentration, temperature and fuel/air ratio in practical combustion systems. *Prog Energy Combust Sci* 31(1):75–121
- Shi L, Mao X, Jaworski J (2010) Application of planar laser-induced fluorescence measurement techniques to study the heat transfer characteristics of parallel-plate heat exchangers in thermoacoustic devices. *Meas Sci Tech* 21(11):115405
- Slipchenko MN, Miller JD, Roy S, Gord JR, Danczyk SA, Meyer TR (2012) Quasi-continuous burst-mode laser for high-speed planar imaging. *Opt Lett* 37(8):1346–1348
- Smith SH, Mungal MG (1998) Mixing structure and scaling of the jet in crossflow. *J Fluid Mech* 357:83–122
- Smith JD, Sick V (2005a) Crank-angle resolved imaging of biacetyl laser-induced fluorescence in an optical internal combustion engine. *Appl Phys B* 81(5):579–584
- Smith JD, Sick V (2005b) High-speed fuel tracer fluorescence and OH radical chemiluminescence imaging in a spark-ignition direct-injection engine. *Appl Opt* 44(31):6682–6691
- Smith JD, Sick V (2007) Quantitative dynamic fuel distribution measurements in combustion-related devices using laser-induced fluorescence imaging of biacetyl in iso-octane. *Proc Combust Inst* 31(1):747–755
- Su LK, Clemens NT (2003) The structure of fine-scale scalar mixing in gas-phase planar turbulent jets. *J Fluid Mech* 488:1–29
- Sutton JA, Driscoll JF (2002) Scalar dissipation rate measurements in flames: a method to improve spatial resolution by using nitric oxide PLIF. *Proc Combust Inst* 29(2):2727–2734
- Sutton JA, Driscoll JF (2006) A method to simultaneously image two-dimensional mixture fraction, scalar dissipation rate, temperature, and fuel consumption rate in a turbulent non-premixed flame. *Exp Fluids* 41(4):603–627
- Sutton JA, Driscoll JF (2013) Measurements and statistics of mixture fraction and scalar dissipation rates in turbulent non-premixed jet flames. *Combust Flame* 160(9):1767–1778
- Tacina KM, Dahm WJA (2000) Effects of heat release on turbulent shear flows. Part 1. A general equivalence principle for non-buoyant flows and its application to turbulent jet flames. *J Fluid Mech* 415:23–44
- Tait NP, Greenhalgh DA (1992) 2D laser induced fluorescence imaging of parent fuel fraction in nonpremixed combustion. *Proc Combust Inst* 24:1621–1628
- Thurber MC (1999) Acetone laser-induced fluorescence for temperature and multiparameter imaging in gaseous flows. Ph. D. Dissertation, Stanford University
- Thurber MC, Hanson RK (1999) Pressure and composition dependence of acetone laser-induced fluorescence with excitation at 248, 266 and 308 nm. *Appl Phys B* 69:229–240
- Thurber MC, Hanson RK (2001) Simultaneous imaging of temperature and mole fraction using acetone planar laser-induced fluorescence. *Exp Fluids* 30(1):93–101
- Thurber MC, Grisch F, Kirby BJ, Votsmeier M, Hanson RK (1998) Measurements and modeling of acetone laser-induced fluorescence with implications for temperature-imaging diagnostics. *Appl Opt* 37:4963–4978
- Thurow B, Jiang N, Samimy M, Lempert WR (2004) Narrow-linewidth megahertz-rate pulse-burst laser for high-speed flow diagnostics. *Appl Opt* 43(26):5064–5073
- Wallington TJ, Kurylo MJ (1987) Flash photolysis resonance fluorescence investigation of the gas-phase reactions of hydroxyl radicals with a series of aliphatic ketones over the temperature range 240–440 K. *J Phys Chem* 102(24), 91(19):5050–5054
- Weber C, Haehn N, Oakely J, Rothamer D, Bonazza R (2012) Turbulent mixing measurements in the Richtmyer-Meshkov instability. *Phys Fluids* 24(7):074105
- Weinkauff J, Trunk P, Frank JH, Dunn MJ, Dreizler A, Böhm B (2015) Investigation of flame propagation in a partially premixed jet by high-speed-Stereo-PIV and acetone PLIF. *Proc Combust Inst* 35:3773–3781
- Wermuth N, Sick V (2005) Absorption and fluorescence data of acetone, 3-pentanone, biacetyl, and toluene at engine-specific combinations of temperature and pressure. SAE Technical Paper 2005-01-2090. doi:10.4271/2005-01-2090
- White FM, Corfield I (2006) *Viscous fluid flow*, vol 3. McGraw-Hill, New York
- Williams B, Ewart P, Wang X, Stone R, Ma H, Walmsley H, Cracknell R, Stevens R, Richardson D, Fu H, Wallace S (2010) Quantitative planar laser-induced fluorescence imaging of multi-component fuel/air mixing in a firing gasoline-direct-injection engine: Effects of residual exhaust gas on quantitative PLIF. *Combust Flame* 157(10):1866–1878
- Wollenhaupt M, Carl SA, Horowitz A, Crowley JN (2000) Rate coefficients for reaction of OH with acetone between 202 and 395 K. *J Phys Chem A* 102(24), 104(12), 2695–2705
- Wu S, Blake GA, Sun S, Ling J (2000) A multicrystal harmonic generator that compensates for thermally induced phase mismatch. *Opt Comm* 173(1):371–376
- Wynanski I, Fiedler H (1969) Some measurements in the self-preserving jet. *J Fluid Mech* 38(03):577–612
- Yuen L, Peters J, Lucht R (1997) Pressure dependence of laser-induced fluorescence from acetone. *Appl Opt* 36:3271–3277
- Zahrada D, Parziale NJ, Smith MS, Marineau EC (2016) Krypton tagging velocimetry in a turbulent Mach 2.7 boundary layer. *Exp Fluids*. 57:62